

“S-Scheme ternary Mxene/ α -Fe₂O₃/CdS photocatalyst: A promising route for sustainable H₂ production”



By

Munazza Sheikh

Reg. NO. 00000365280

This thesis is submitted as partial fulfillment of requirements for the degree of

MASTER OF SCIENCE IN

CHEMISTRY

Supervised By: Dr. Shahid Iqbal

**Department of Chemistry, School of Natural Sciences,
National University of Sciences and Technology, (NUST),**

Islamabad, Pakistan.

2023

THESIS ACCEPTANCE CERTIFICATE

Certified that final copy of MS thesis written by Munazza Sheikh (Registration No. 00000365280), of School of Natural Sciences has been vetted by undersigned, found complete in all respects as per NUST statutes/regulations, is free of plagiarism, errors, and mistakes and is accepted as partial fulfillment for award of MS/M.Phil degree. It is further certified that necessary amendments as pointed out by GEC members and external examiner of the scholar have also been incorporated in the said thesis.


Signature: 

Name of Supervisor: Dr. Shahid Iqbal

Date: 11/08/2023

Signature (HoD): 

Date: 11/08/2023

Signature (Dean/Principal): 

Date: 11-08-2023

National University of Sciences & Technology**MS THESIS WORK**

We hereby recommend that the dissertation prepared under our supervision by: **Munazza Sheikh**, Regn No. **00000365280** Titled: "**S-scheme ternary Mxene/ α -Fe₂O₃/CdS Photocatalyst: A Promising Route for Sustainable H₂ Production**" accepted in partial fulfillment of the requirements for the award of **MS** degree.


Examination Committee Members1. Name: PROF. MANZAR SOHAILSignature: 2. Name: DR. MUHAMMAD ADIL MANSOORSignature: Supervisor's Name: DR. SHAHID IQBALSignature: 
Head of Department11/08/2023
Date**COUNTERSIGNED**Date: 11.08.2023
Dean/Principal

Table of Figures

Figure 1: H ₂ Production from different photocatalysts[11].....	3
Figure 2: Type I and Type II heterojunctions[35]	7
Figure 3: Zero Dimensional materials[42].....	9
Figure 4: One Dimensional materials	10
Figure 5: 2D materials and their properties[46].....	10
Figure 6: Graphene A 2D material for H ₂ Production[48]	11
Figure 7 : Proposed mechanism for MoS ₂ /CdS[50].....	12
Figure 8 : Doped Graphene for efficient water splitting[56]	14
Figure 9: Conduction and Valence band structure of CdS[60]	15
Figure 10 : Band structure of α -Fe ₂ O ₃ [68].....	17
Figure 11 : Mxene for photocatalysis water splitting[70]	18
Figure 12 : α -Fe ₂ O ₃ and CdS Band structure[79]	22
Figure 13: Mechanism of photocatalytic water splitting[83].....	24
Figure 14: Synthesis of 2D CdS.....	30
Figure 15: Synthesis of α -Fe ₂ O ₃ BY SOLVOTHERMAL METHOD.....	31
Figure 16 :Synthesis of Mxene by etching	32
Figure 17 : Fabrication of Ternary Heterojunction	34
Figure 18: Xrd of CdS, α -Fe ₂ O ₃ , Max and Mxene	36
Figure 19: XRD of Binary and Ternary heterojunctions.....	37
Figure 20 : a) XPS survey b) Fe2p c) Ti2p d) O1s	38
Figure 21: XPS of e) C1s f) Cd3d g) S2p	40
Figure 22: SEM images of a-b) α -Fe ₂ O ₃ , c-e) CdS , f-g) α -Fe ₂ O ₃ /CdS.....	41

Figure 23: TEM images of Mxene.....	42
Figure 24: EDS spectra of CdS and α -Fe ₂ O ₃	42
Figure 25: EDS spectra of Binary composite	43
Figure 26: UV-Vis Spectroscopy	44
Figure 27: Band-Gaps from Tauc plots.....	45
Figure 28: PL spectra	46
Figure 29: H ₂ Evolution rate of different binary heterojunction ratio	47
Figure 30: H ₂ evolution rates of different concentration of Mxene loaded	48
Figure 31: H ₂ production over different sacrificial reagents	49
Figure 32 : CA at 0.5V DC supply.....	50
Figure 33: Mechanism of photocatalytic water splitting showing C-B, V-B and Fermi level.....	52

Table of Contents

1	Introduction:.....	1
1.1	Heterojunctions photocatalysis	4
1.2	Types of heterojunctions	6
1.2.1	Type-I Heterojunction.....	6
1.2.2	Type-II Heterojunction.....	7
1.3	Types of materials	8
1.3.1	0D materials (nanoparticles or quantum dots).....	8
1.3.2	One-dimensional (1D) materials.....	9
1.3.3	2D- dimensional materials	10
1.3.4	Types of 2D Materials.....	11
1.4	1D-1D Materials:.....	13
1.4.1	Semiconducting nanowires and metal nanowires:	13
1.5	2D-2D Materials.....	14
1.5.1	Transition metal dichalcogenides (TMDs) and graphene	14
1.5.2	Hexagonal boron nitride (h-BN) and graphene:	14
1.5.3	2D-2D CdS and Mxene.....	15
1.5.4	α -Fe ₂ O ₃ and Mxene	16
1.6	Ternary Heterojunction Photocatalyst:.....	18
1.6.1	Design of the Ternary Heterojunction Photocatalyst:	18

1.6.2	Effects:	18
1.6.3	Examples of ternary heterojunctions:	19
1.6.4	CdS/ α -Fe ₂ O ₃ /Mxene:	20
1.7	Mechanism of photocatalytic water splitting	21
1.7.1	Photon Absorption:	21
1.7.2	Photogenerated Charge Separation:	22
1.7.3	Charge diffusion and transport.....	22
1.7.4	Catalytic Reactions at the Active Sites of the Catalyst:	23
1.7.5	Mass Transfer:.....	23
2	Literature Survey:	31
3	Synthesis:	36
4	Characterization:	41
5	Applications:.....	53
6	Conclusions:.....	59
7	References:.....	60

بِسْمِ اللَّهِ الرَّحْمَنِ الرَّحِيمِ

Dedication

*Dedicated To My Unwavering Pillars of Support, My
Beloved Parents.*

Statement of Original Authorship

I, **Munazza Shiekh** hereby state that my MS thesis titled "**S-SCHEME TERNARY Mxene/Fe₂O₃/CdS PHOTOCATALYST: A PROMISING ROUTE FOR SUSTAINABLE H₂ PRODUCTION**" is my work and has not been submitted previously by me for taking any degree from National University of Science and Technology or anywhere else. At any time if my statement is found to be incorrect even after I've graduated, the university has the right to withdraw my MS degree.

Name of Student: **Munazza Shiekh**

ACKNOWLEDGEMENT:

I want to express my sincere gratitude and appreciation to everyone who helped me along the way to finishing my master's in chemistry thesis. I want to start by saying how grateful I am to my research supervisor, **Dr. Shahid Iqbal**, for their unflinching advice, priceless insights, and ongoing support. Their knowledge and commitment have been crucial in forming this research.

I owe a debt of gratitude to my GEC members **Dr. Manzar Sohail** and **Dr. Adil Mansoor** for their lectures, roundtable discussions, and for creating a stimulating learning atmosphere. Their dedication to perfection has served as a constant inspiration.

My deepest gratitude goes out to my family, my husband **Mr. Hanan** and friends for their unfailing support and patience. Their emotional and practical support has been crucial in helping me overcome obstacles and maintain my motivation. In addition, I want to express my gratitude to my research associates and other students who contributed their knowledge and fostered a supportive environment that improved the caliber of my work.

Last but not least, I'd like to thank everyone who took part in this study and say how much I appreciate it. Their assistance was essential to my research's success. I would like to conclude by expressing my sincere gratitude to **Sadam Hussain** who helped shape my thesis and supported me in my academic endeavors. Your assistance has been genuinely priceless.

Munazza Sheikh

ABSTRACT

Here, a novel synthesis of Mxene/ α -Fe₂O₃/CdS step-scheme (S-scheme) hybrid heterojunction with cascade 2D coupling interfaces was purposefully fabricated using hydrothermal techniques. Through in-situ irradiation XPS, or UV-Visible Spectroscopy investigations, the building of S-scheme was discovered, which may significantly increase the photocatalytic H₂ evolution reaction (HER) rate and stability. In comparison to pure CdS nanosheets (NSs), the H₂ evolution rates of Mxene/ α -Fe₂O₃/CdS were, respectively higher. The maximum HER activity measured in the optimized ternary composite is 51.04 mmol g⁻¹ h⁻¹ at 450 nm. The ternary photocatalyst, however, continued to show substantially higher stability. Without a doubt, the strong S-scheme interfacial electric fields could efficiently promote spatial charge separation between CdS nanosheets and α -Fe₂O₃ nanosheets, while 2D Mxene nanosheets, as H₂-evolution co-catalyst, could offer more electron transfer pathways and a significant number of active sites for photocatalytic HER. This work is anticipated to provide some fresh ideas or inspirations for the rational design of extremely effective S-scheme heterojunction photocatalysts for more practical applications

1. Introduction:

The current era necessitates the expeditious advancement of renewable energy sources to cater to the demand for enduring and copious energy, given the exhaustion of non-renewable fossil fuels such as coal, natural gas, and petroleum oil[1]. The exploration of novel methodologies and advanced technologies for the acquisition of renewable energy has gained significant importance in recent times[2]. One of the more promising methods entails the transformation of solar energy into chemical energy, sometimes known as "solar fuels." Solar fuels include hydrogen (H₂), methanol, methane, and other energy-storing and -releasing substances[3].

The development of a low-carbon emission economy is usually seen as benefiting greatly from the availability of hydrogen as an energy source. To start, it's crucial to remember that hydrogen has a substantially higher calorific value per unit of mass than natural gas or gasoline, by a factor of four and three, respectively. Due of its ability to burn without producing greenhouse gases, hydrogen demonstrates environmental friendliness. Solar energy storage using hydrogen is usually regarded as the best strategy for creating sustainable and environmentally friendly energy systems[4]. Furthermore, hydrogen exhibits a ubiquitous presence in a diverse range of chemical compounds and holds the distinction of being the most abundant element in the cosmos. Due to its high accessibility and versatile nature, hydrogen exhibits significant potential as a flexible and convenient energy resource[5]. Thirdly, hydrogen serves as a crucial chemical reagent employed in diverse industrial operations. Extensive research has been conducted on the subject of photocatalytic or photoelectrochemical (PEC) water splitting, a process that harnesses solar energy to facilitate the separation of water molecules into hydrogen and oxygen components. The significance of fostering a hydrogen-based economy stems from its pivotal role in the realm of technological advancement. A significant milestone in this domain was the seminal research

conducted by Fujishima and Honda on the photoelectrochemical water splitting reaction employing a titanium dioxide (TiO_2) electrode[6]. Since that point in time, a group of scientists and researchers have been actively engaged in conducting thorough investigations on different photocatalytic and PEC (photoelectrochemical) systems. These investigations involve the examination of a wide array of materials and methodologies with the aim of enhancing the efficiency of water splitting and the subsequent production of hydrogen. The objective is to devise cost-effective and ecologically sustainable methodologies for large-scale hydrogen production utilizing renewable energy sources, such as solar power[7].

In summary, the conversion of solar energy into chemical energy, specifically hydrogen, has emerged as a highly auspicious approach for addressing the forthcoming energy and environmental challenges. The progress of clean and sustainable energy solutions is contingent upon the ongoing research and development efforts in the fields of photocatalytic and photoelectrochemical water splitting[8]. In order to solve water, air, and soil contamination, researchers and scientists have invested enormous effort in inventing environmentally friendly products and practices. All life forms depend on water, so it needs to be carefully managed and purified[9]. Wastewaters from factories, businesses, and research facilities are important sources of pollution because they include a variety of poisonous compounds that are bad for both people and the environment, including organic poisons, dyes, heavy metals, pesticides, and herbicides[10].

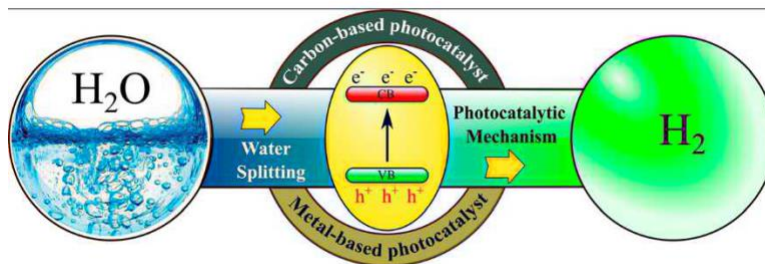


Figure 1: H₂ Production from different photocatalysts[11]

An issue that affects the entire world is water contamination. Significant water pollution has been caused by human activities and industrial development, endangering human health. It is essential for societal and economic well-being in all sectors to have access to clean water and sanitary facilities[12]. Unfortunately, the amount of biological, chemical, and microbiological pollutants in water is rising as a result of human activity. Agriculture, unintentional oil spills, poor domestic and industrial waste disposal, as well as numerous chemical-intensive industrial processes, are all sources of contamination[13].

Chemicals such as dyes and heavy metals represent significant environmental risks and can have negative health effects. With the objective of discovering efficient and long-lasting solutions to lessen the negative effects on ecosystems, human health, and general well-being, efforts to reduce water pollution are still being made. Due to a lack of automatic cleaning systems, inadequate industrial waste treatment, and the manufacture of dangerous chemicals, water contamination has escalated into a serious problem. Therefore, there is a critical need for pollution prevention and management measures that are practical, cheap, and have no negative influence on the environment or human health[14].

Through the splitting of water molecules, photocatalytic water splitting is a method for transforming solar energy into hydrogen fuel[15]. Since hydrogen is a clean energy source and produces only water as a byproduct when utilized in fuel cells, this technology is regarded as being environmentally benign[16]. This substance takes in photons of light energy and uses them to fuel the water splitting reaction, which would otherwise be thermodynamically unfavorable. Different photoactive materials that satisfy specified requirements for effective solar energy conversion through water splitting are being actively researched by researchers[17].

The majority of single photocatalyst compounds, however, have drawbacks. They either exhibit photo corrosion to a large degree or are only active in the ultraviolet (UV) band of light. Recombination of photoexcited charges is another difficulty because it lowers the overall effectiveness of water splitting[19]. Researchers have been investigating the idea of creating heterostructures to overcome these restrictions. In order to do this, many functional elements must be combined inside of a single photocatalyst. Because it enables the combination of desirable features from each contributing chemical. The effectiveness of splitting of water can be increased by expanding range to encompass light, decreasing the recombination of photoexcited e-h pairs, boosting photo corrosion stability, and creating heterostructures[20].

Diverse photoactive materials are being actively researched, and the creation of heterostructures has the potential to go beyond the constraints of single photocatalyst materials and increase the effectiveness of the water splitting process[21].

1.1 Heterojunctions photocatalysis

The ability of single photocatalyst materials to split water has been extensively explored, however these materials frequently have drawbacks such being active only under ultraviolet (UV) light or having a lot of photo corrosion. Recombination of photoexcited charges is another issue that lowers

the overall effectiveness of water splitting[22]. Researchers have turned to the idea of creating heterostructures by fusing various functional materials inside of a single photocatalyst to get around these limits. This strategy has a tremendous deal of potential for solving the problems with single photocatalyst materials[23]. The advantageous characteristics of each involved component can be synergistically combined by forming heterostructures. This enables the visible spectrum to be included in the absorption range, increasing the efficiency of solar energy usage beyond merely UV radiation. A greater solar spectrum can be captured by the heterostructures with a wider range of absorption, enhanced efficiency.[24].

Additionally, the rejoining of photoexcited e-h pairs is decreased via development of heterojunctions. Recombination wastes energy and reduces the effectiveness process, hence preventing it is essential. These can increase the separation and use of charge transporters by minimizing recombination, which boosts overall performance[25]. Additionally, adding various materials to heterostructures can improve the photocatalyst's resilience against photo corrosion. The degradation or loss of catalytic activity brought on by extended exposure to light is referred to as photo corrosion. The stability and longevity of the photocatalyst can be increased, assuring its long-term efficacy in water splitting, by selecting materials with better photo corrosive resistivity[26]. A viable method of overcoming the drawbacks of single photocatalyst materials is the development of heterostructures by fusing many functional elements within a single photocatalyst. The absorption range can be expanded, charge carrier recombination can be reduced, photo corrosive stability can be improved, and this all contributes to higher water splitting efficiency[27].

To obtain the necessary qualities for a water splitting photocatalyst, there are significant challenges in developing and producing heterostructures employing a variety of functional materials. When

creating a heterojunction, it is crucial to ensure that the levels of energy of the coupled materials are closely related and have matching of band structure[28].

1.2 Types of heterojunctions

1.2.1 Type-I Heterojunction

In a type I heterojunction, h transfer to the less positively charged V-B of the material, whilst electrons migrate to the less negatively charged band for conduction. It also lowers the redox capacity of the photoexcited charges after they have gone through the heterojunction[29]. In a Type I heterojunction, a heterostructure combining an (OEC) and a hydrogen evolution photocatalyst (HEC) is used to split water. Electrons and holes that have been photoexcited can move across the heterojunction contact because the two materials' band boundaries overlap[30].

When lighted by photons, the HEC material's V-B offers upper positive energy level compared to the OEC material's V-B, and the OEC material's C-B is positioned more negatively than the HEC material's conduction band. Due to this energy band alignment, photoexcited e^- move from the HEC material to the OEC material and holes move in the other manner. The effective charge separation and improved redox reactions brought about by the transfer of photoexcited e^- and holes through this heterojunction. In the reduction and oxidation reactions, which result in the formation of hydrogen and oxygen, respectively, the transported electrons and holes can take part[31].

The band offset, Type I heterojunctions offer benefits such improved charge separation and decreased charge recombination. The ability to expand light absorption to a wider region of the solar spectrum and to reduce charge recombination may be restricted in Type I heterojunctions as compared to Type II heterojunctions[32].

1.2.2 Type-II Heterojunction

In the context of water splitting for photocatalysis, a Type II heterojunction is a particular configuration of a heterojunction structure. The V-B and C-B of the involved materials are aligned at staggered energies in a Type II heterojunction. For applications involving water splitting, this design permits effective charge separation and transfer[33].

A Type II heterojunction typically comprises of two different semiconducting materials, each with a unique band gap energy, in the context of water splitting. The oxygen evolution photocatalyst (OEC) facilitates the oxidation reaction that results in oxygen (O_2), whereas the hydrogen evolution photocatalyst (HEC) facilitates the reduction reaction that results in hydrogen (H_2). In a Type II heterojunction, the staggered energy band alignment results in spatially separated charge carriers, with electrons building up in one material and holes building up in the other[34].

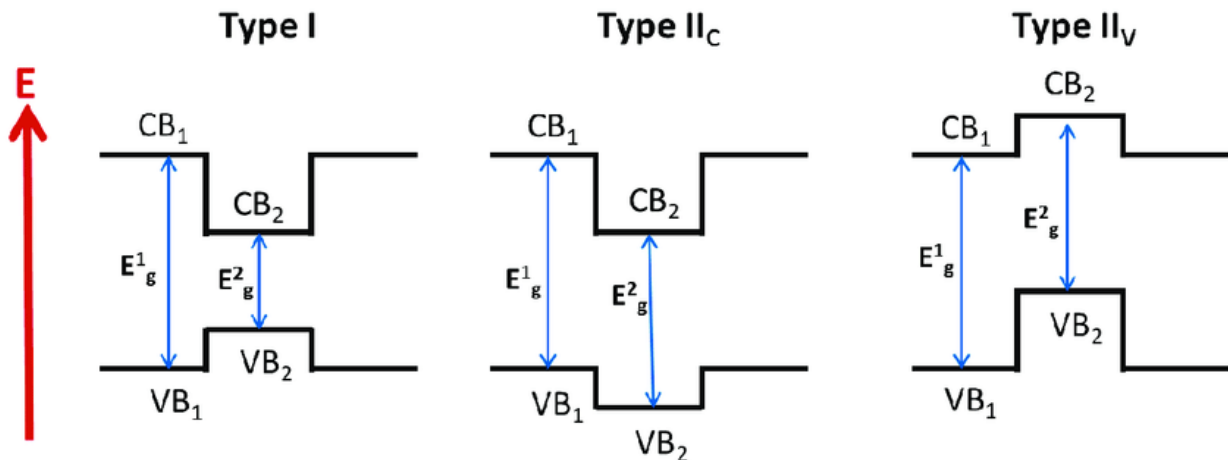


Figure 2: Type I and Type II heterojunctions[35]

Compared to a single photocatalyst material, the Type II heterojunction absorbs light energy over when photons are present. In both materials, the photons excite electrons to move from the V-B to C-B. The photoexcited electrons tend to migrate from the sample with a higher C-B position to the material with a lower C-B position as a result of the staggered band alignment, whereas the

holes migrate in the other direction. By efficiently suppressing charge recombination, this charge separation raises the overall effectiveness of water splitting[36].

For water splitting, the Type II heterojunction architecture offers a number of benefits. It maximizes the use of solar energy by extending light absorption to a wider range, including visible light. The reduction in recombination spatial makes the charge transfer for the corresponding reduction and oxidation reactions involved in water splitting more effective. Overall, Type II heterojunctions present a sustainable strategy for improving the performance of hydrogen and oxygen synthesis by boosting, which will increase the efficiency of water splitting photocatalysis[37]. Carefully planning and constructing heterostructures, scientists are aiming to enhance charge separation and transfer, maximize the usage of visible light, and raise the efficiency of water splitting reactions[38].

1.3 Types of materials

1.3.1 0D materials (nanoparticles or quantum dots)

Materials that are zero-dimensional (0D) and one-dimensional (1D) have a lot of interest because of their potential uses in water splitting, notably as photocatalysts. These substances have special structural and physical qualities that can improve the effectiveness of the water splitting process. 0D materials, sometimes referred to as nanoparticles or quantum dots, are nanoscale objects with dimensions typically between a few and a few tens of nanometers. A high surface-to-volume ratio in these materials improves the exposure of active areas for catalytic processes[39]. 0D materials can function as effective photocatalysts in this process because of their tunable band gaps, which permit the absorption of a wide range of photons, including visible light. Researchers can precisely tune the optical characteristics and energy band topologies of 0D nanoparticles for effective charge separation and increased catalytic activity[40]. Applications for water splitting have been

investigated using a variety of 0D materials, including metal oxides (such as titanium dioxide nanoparticles), metal sulphides, and C based nanomaterials (such as graphene quantum dots). These materials provide effective solar energy utilization for water splitting reactions thanks to their high surface area, superior stability, and tunable surface chemistry[41].

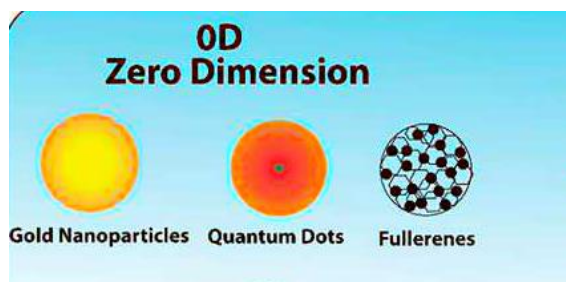


Figure 3: Zero Dimensional materials[42]

1.3.2 One-dimensional (1D) materials

One-dimensional (1D) materials have an extended structure along one axis while retaining nanoscale dimensions in the other two axes. Nanowires, nanorods, nanotubes, and nanofibers are a few types of 1D materials[43]. Due to their high aspect ratio and constrained geometries, 1D materials have special features. These characteristics, which are all essential for photocatalytic water splitting, include better charge transport, and effective charge separation. Researchers can boost the photocatalytic efficiency of 1D materials by optimizing their crystal structures, surface characteristics, and doping. By improve the use of water splitting, semiconducting metal oxide nanowires like CdS, TiO₂, ZnO, or hematite (α -Fe₂O₃) nanowires have been studied for their effective charge transfer and enhanced light absorption[44].

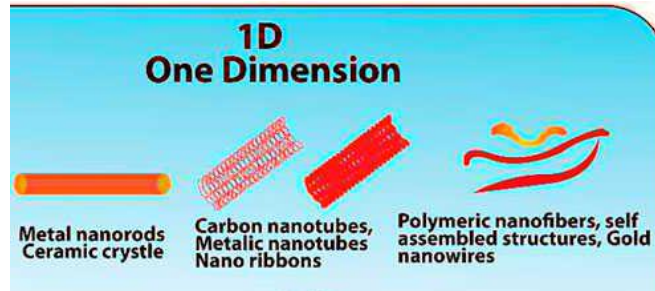


Figure 4: One Dimensional materials

1.3.3 2D- dimensional materials

Due to their remarkable characteristics and atomic-scale thickness, two-dimensional (2D) materials have suited intriguing candidates for the creation of hydrogen (H₂). These substances, which are made of one or more layers of atoms, have special electrical, optical, and catalytic properties that make them promising for the synthesis of H₂[45].

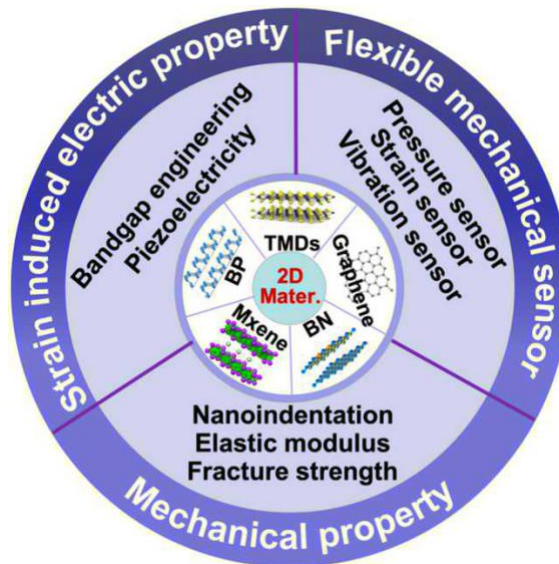


Figure 5: 2D materials and their properties[46]

1.3.4 Types of 2D Materials

1.3.4.1 Graphene

It is a sheet of hexagonally structured carbon atoms that exhibits exceptional electrical conductivity. Graphene oxide (GO) and nitrogen-doped graphene, two derivatives and modifications of pure graphene, have demonstrated potential as co-catalysts for accelerating H₂ evolution processes (HER), despite pristine graphene's ineffectiveness as a catalyst for H₂ synthesis. To increase the overall effectiveness of H₂ production, these graphene-based materials can be coupled with additional catalysts[47].

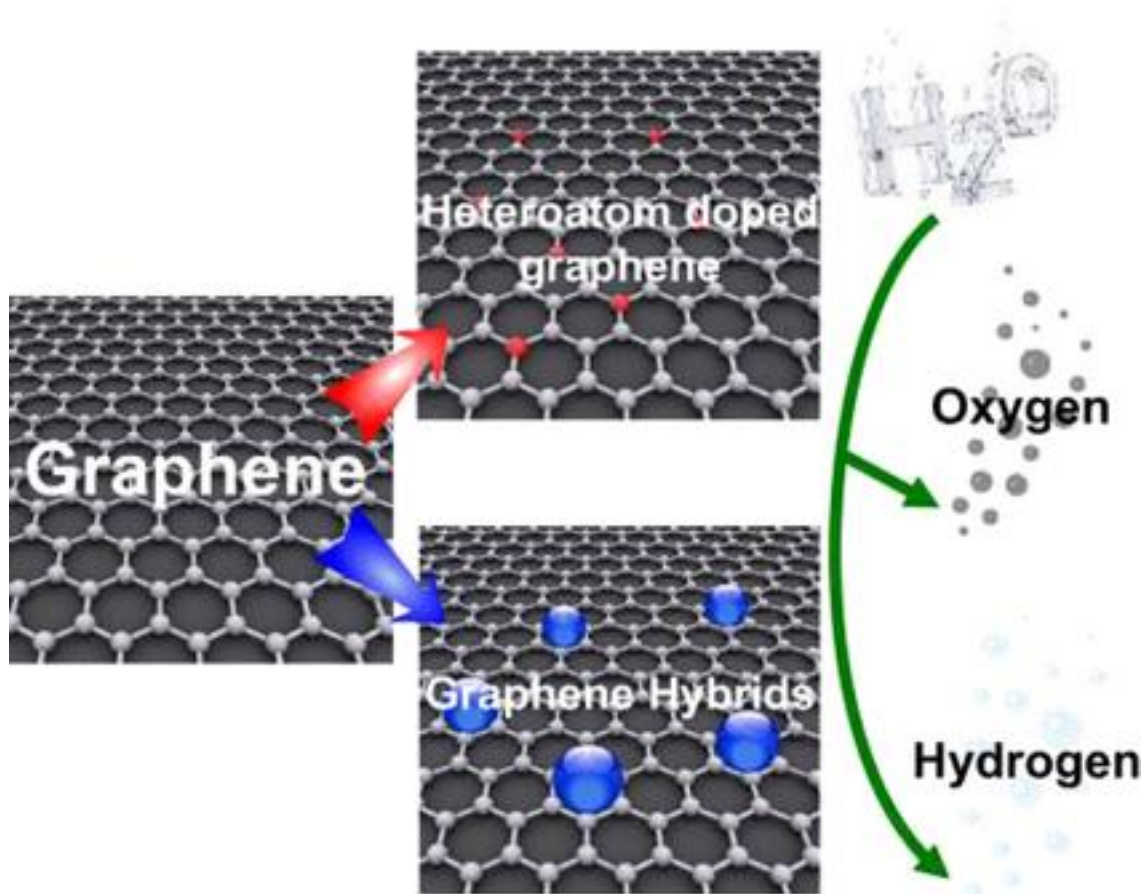


Figure 6: Graphene A 2D material for H₂ Production[48]

1.3.4.2 Transition Metal Dichalcogenides (TMDs):

Layered compounds with distinct electrical characteristics include tungsten Di selenide (WSe_2) and molybdenum disulfide (MoS_2). Both the HER and the (OER) are catalyzed by them. TMDs have synergistic effects that increase the overall effectiveness of water splitting and can be utilized as standalone catalysts or combined with other substances to generate heterostructures[49].

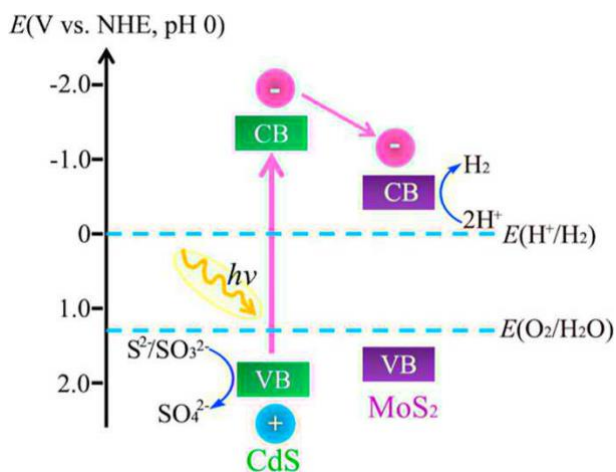


Figure 7 :Proposed mechanism for MoS_2/CdS [50]

1.3.4.3 Black Phosphorus:

Also known as phosphorene, (BP) is a 2D substance with a puckered structure. BP's favorable bandgap for visible light absorption has made it a promising photocatalyst for the synthesis of H_2 . BP's distinctive electronic structure makes it possible for effective charge separation and transfer, which boosts its catalytic activity for splitting water[51].

1.3.4.4 Hexagonal Boron Nitride (h-BN):

Outstanding in both thermal and chemical stability, is a 2D insulating material. Even though h-BN alone lacks catalytic activity for water splitting, it can support or act as a shield for other catalyst materials. The total efficiency of H_2 production is increased by coating metal or

semiconductor catalysts with h-BN to assist avoid corrosion and degradation and extend their catalytic effectiveness[52].

These are just a handful of the 2D materials that are being investigated for H₂ generation. High surface area, customizable electronic structure, and catalytic activity are just a few of the distinctive qualities that make 2D materials fascinating candidates for boosting the effectiveness of H₂ evolution reactions in water splitting processes. In order to fully realize these materials' promise for sustainable H₂ production, research is still being done to further optimize them and create new production methods.

Certainly! Combinations of 1D-1D and 2D-2D materials have been studied for the creation of hydrogen (H₂), taking advantage of each material's special characteristics to improve catalytic performance. Examples of these combinations are as follows:

1.4 1D-1D Materials:

Metal oxide nanowires and carbon nanotubes (CNTs) Metal oxide nanowires can be supported or scaffolded by CNTs, which offer strong electrical conductivity and a sizable surface area. Combining the two improves charge transfer and makes H₂ evolution reactions more productive. For instance, CNTs with tungsten trioxide (WO₃) or titanium dioxide (TiO₂) nanowires have demonstrated increased catalytic activity for the generation of H₂[53].

1.4.1 Semiconducting nanowires and metal nanowires:

Synergistic effects can be attained by mixing semiconducting nanowires (like silicon, germanium, or III-V compound semiconductors) with metal nanowires (like platinum, palladium, or nickel). While the metal nanowires serve as effective catalysts for H₂ evolution, the semiconducting

nanowires absorb light and produce charge carriers. The combination improves charge separation and catalytic activity, which increases the effectiveness of H₂ synthesis[54].

1.5 2D-2D Materials

1.5.1 Transition metal dichalcogenides (TMDs) and graphene

are examples of two-dimensional materials Heterostructures can be created using graphene and TMDs like tungsten Di selenide (WSe₂) or molybdenum disulfide (MoS₂). These materials' distinctive band topologies make efficient charge transfer possible and boost catalytic activity. Charge separation and H₂ evolution reactions are facilitated and supported by the interfaces between graphene and TMDs. In comparison to individual materials, these heterostructures have demonstrated better performance in the generation of H₂[55].

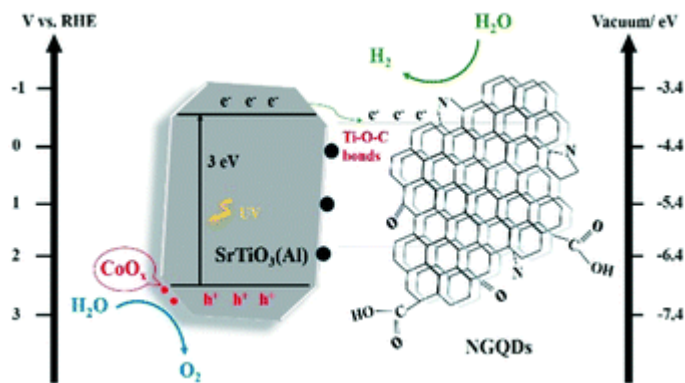


Figure 8 :Doped Graphene for efficient water splitting[56]

1.5.2 Hexagonal boron nitride (h-BN) and graphene:

Graphene's stability is improved and its corrosion is stopped by the protective layering effect of h-BN. Improved H₂ generation efficiency results from the combination of graphene with h-BN, which maintains the outstanding electrical conductivity and catalytic activity of graphene while providing chemical stability and protection[57].

1.5.3 2D-2D CdS and Mxene

For effective water splitting, the combination of 2D cadmium sulphide (CdS) with MXene as a photocatalyst for hydrogen (H₂) production has shown excellent properties.

CdS is a viable choice for photocatalytic applications because it is a semiconductor material with a bandgap that is appropriate for absorbing visible light[58]. On the other hand, it is a class of layered 2D transition metal carbides, nitrides, or carbonitrides. The combination of CdS and MXene results in the formation of a heterostructure, which capitalizes on the distinctive properties of both materials for process of water splitting. The utilization of a CdS/MXene heterostructure for the synthesis of H₂ offers several advantageous features[59].

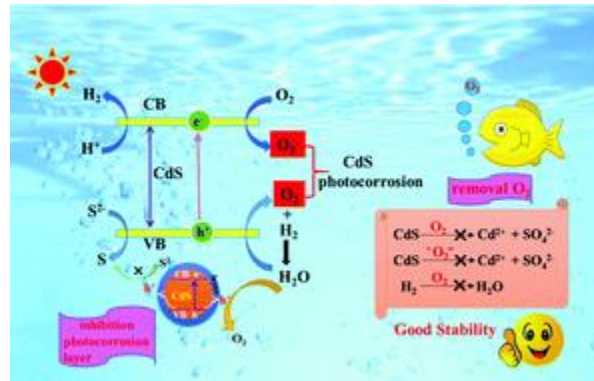


Figure 9: Conduction and Valence band structure of CdS[60]

1.5.3.1 Advantages of CdS/Mxene photocatalyst for water splitting

1.5.3.1.1 Increased Light Absorption:

MXene can help to broaden the range of visible light that CdS can absorb because of its wider bandgap. This broader light absorption range increases the efficiency of H₂ generation and the use of solar energy[61].

1.5.3.1.2 Effective Charge Separation and Transfer:

In response to illumination, CdS produces photoexcited electrons, while MXene offers channels for effective charge separation and transfer. Increased catalytic activity results from the spatial separation of charge carriers because it reduces recombination and lengthens the lifespan of separated charges[62].

1.5.3.1.3 Cocatalytic Effects:

Materials made of MXene can also act as cocatalysts, accelerating surface reactions and streamlining the entire water splitting procedure. The activity and durability of the heterostructure can be improved by MXenes' high electrical conductivity and variable surface chemistry[63].

Optimizing the interfacial characteristics and improving the overall photocatalytic performance for H₂ production are the goals of the careful synthesis and integration of the components. While the heterostructure formed by CdS and MXene shows promise for the production of H₂, more investigation and optimization of composition, structure, and interface engineering methodologies are still being pursued. Through photocatalytic water splitting, these initiatives seek to enhance charge separation, boost catalytic effectiveness, and produce H₂ in an efficient and sustainable manner[64].

1.5.4 α -Fe₂O₃ and Mxene

The α -Fe₂O₃ compound is a semiconductor photocatalyst that has garnered significant attention in academic research. It exhibits characteristics of an extrinsic semiconductor, with a relatively narrow E_g of approximately 2.1 electron volts (eV). Notably, it demonstrates exceptional responsiveness to visible light, making it highly desirable for photocatalytic applications[65]. Additionally, α -Fe₂O₃ possesses a range of appealing properties, including various morphologies, favorable thermodynamic stability, affordability, abundant availability in nature, and

environmental compatibility. Nevertheless, the catalytic performance of α -Fe₂O₃ is deemed unsatisfactory, prompting the exploration of this photocatalytic system as a potent approach to enhance its activity. Schottky junctions rely significantly on the utilization of precious metal materials[66]. In theory, if the work function of a metal is greater than that of iron oxide, it is possible to establish a Schottky junction at their contact interfaces. This junction effectively hinders the backward movement of photogenerated electrons that have been trapped by the metal. Nevertheless, the exorbitant expense associated with precious metals necessitates the exploration of viable alternatives for the fabrication of Schottky-scheme systems[67].

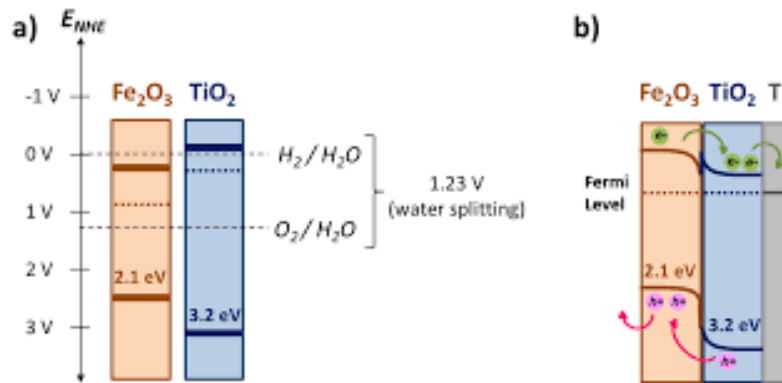


Figure 10 : Band structure of Fe₂O₃[68]

The two-dimensional MXene Ti₃C₂ is undeniably a viable option due to its exceptional conductivity, substantial SA, robust absorption properties, and appropriate Fermi level. In contrast to the conventional accordion-shaped Ti₃C₂, the single-layer MXene exhibits a multitude of advantages. There are several factors that contribute to the enhanced performance of the material under consideration. Firstly, the ultra-thin thickness of the material decreases the distance that carriers need to travel, thereby shortening the carrier migration path. Secondly, the material possesses a unique electronic structure that facilitates efficient electron transfer. Lastly, the material exhibits a large and uniform crystal structure, which exposes numerous active sites that

are nearly identical in nature. Significantly, the appeal of 2D/2D heterojunctions lies in their comparatively area, minimal, and extensively distributed active sites. In light of these factors, the combination of 2D α -Fe₂O₃ hexagonal nanosheets and 2D monolayer MXene Ti₃C₂ nanosheets represents a commendable endeavor in the development of a prospective 2D/2D photocatalyst for hydrogen (H₂) production[69].

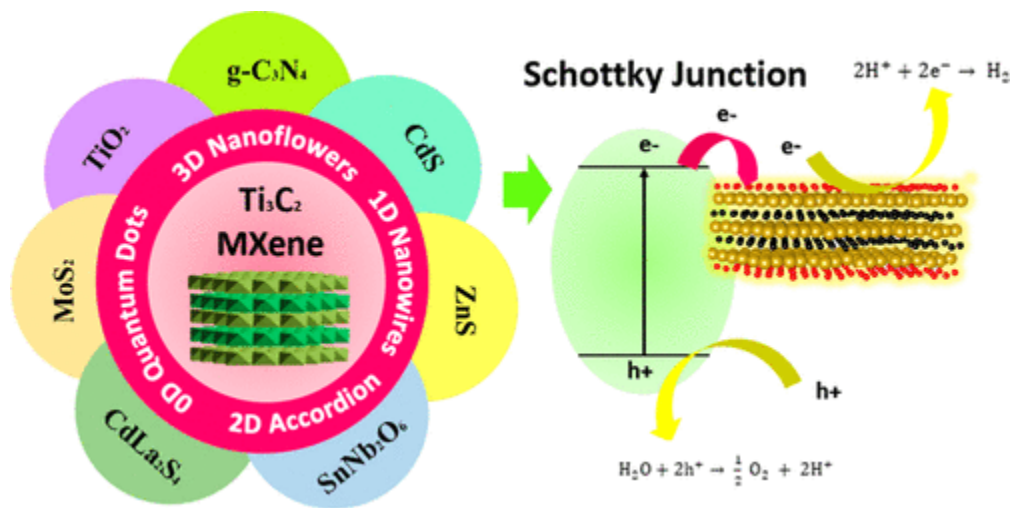


Figure 11 : Mxene for photocatalysis water splitting[70]

1.6 Ternary Heterojunction Photocatalyst:

1.6.1 Design of the Ternary Heterojunction Photocatalyst:

The Ternary Heterojunction Photocatalyst is a three-material system that typically consists of two semiconductors, a cocatalyst, and an electron mediator. The cocatalyst promotes surface reactions and boosts catalytic activity, while the semiconductors absorb light and produce charge carriers[71].

1.6.2 Effects:

The ternary heterojunction makes use of each material's special characteristics to provide synergistic effects that improve the total photocatalytic performance. Higher H₂ generation

efficiency is made possible by the combination's improved charge separation, expanded light absorption range, increased catalytic activity, and decreased charge carrier recombination[72].

Water splitting ternary heterojunction photocatalysts typically combine three different materials, each with unique characteristics and functions. Examples of ternary heterojunction photocatalysts for water splitting include the following:

1.6.3 Examples of ternary heterojunctions:

1.6.3.1 TiO₂/WO₃/BiVO₄:

This ternary heterojunction consists of bismuth vanadate (BiVO₄), titanium dioxide (TiO₂), and tungsten trioxide (WO₃). TiO₂ functions as a photocatalyst with strong stability and a bandgap appropriate for absorbing visible light. Cocatalyst WO₃ enhances surface reactions and charge transfer. The semiconductor BiVO₄ improves light absorption and electron-hole separation. It is a visible light-absorbing material. These components work synergistically together to improve the effectiveness of water splitting[73].

1.6.3.2 CdS/CdSe/TiO₂:

Cadmium sulphide (CdS), cadmium selenide (CdSe), and titanium dioxide (TiO₂) make up this ternary heterojunction. Both the semiconductors CdS and CdSe have adequate bandgaps for absorbing visible light. They produce electron-hole pairs by acting as light absorbers. TiO₂ serves as a cocatalyst to promote surface reactions and charge transfer. Improved catalytic activity and effective charge separation are made possible by the ternary heterojunction structure, which increases the effectiveness of water splitting[74].

1.6.3.3 MoS₂/g-C₃N₄/CdS

Molybdenum disulfide (MoS₂), graphitic carbon nitride (g-C₃N₄), and cadmium sulphide (CdS) are all present in this ternary heterojunction. Layered 2D materials with favorable electrical characteristics for charge separation and transfer include MoS₂ and g-C₃N₄. As a light absorber, CdS is used. These components work together to provide an advantageous band alignment and an effective charge transfer, which enhances the efficiency of water splitting[75].

1.6.3.4 Bi₂WO₆/WO₃/CdS:

The ternary heterojunction in question is composed of tungsten trioxide (WO₃), bismuth tungstate (Bi₂WO₆), and cadmium sulphide (CdS). Visible light and charge separation capabilities are provided by Bi₂WO₆ and WO₃. In order to improve charge transfer and surface reactions, CdS works as a cocatalyst. The charge separation, and catalytic activity of the ternary heterojunction structure lead to increased water splitting efficiency[76].

These examples show how ternary heterojunction photocatalysts can be used to divide water because the three different materials they combine have synergistic effects and enhance overall performance. These photocatalysts have the potential to produce hydrogen efficiently and sustainably through water splitting reactions using solar energy. The performance of ternary heterojunction photocatalysts is currently being improved by the investigation of new material combinations, morphologies, and interface engineering techniques.

1.6.4 CdS/Fe₂O₃/Mxene:

A promising photocatalytic system for producing hydrogen (H₂) through water splitting is the CdS/Fe₂O₃/MXene ternary heterojunction. Cadmium sulphide (CdS), iron (III) oxide (Fe₂O₃), and MXene materials are used in this ternary heterojunction to provide synergistic effects and improve the overall photocatalytic performance.

For H₂ production through water splitting, the combination of these elements in the CdS/Fe₂O₃/MXene ternary heterojunction offers a number of benefits:

1.6.4.1 Extended Light Absorption Range:

Due to their unique bandgaps, CdS and Fe₂O₃ both absorb visible light. Improved solar energy utilization is made possible by the addition of MXene, which increases the range of light absorption.

1.6.4.2 Effective Charge Separation and Transfer:

MXene's presence in the ternary heterojunction promotes separation. As a result, there is less charge recombination, the lifespan of isolated charge carriers is increased, and photoexcited electrons and holes are used more effectively.

1.7 Mechanism of photocatalytic water splitting

The process of water splitting is characterized by a thermodynamically unfavorable reaction, which necessitates an input of energy greater than 1.23 electron volts (eV) in order to proceed. Due to the requirement of four binding sites for each oxygen molecule, the process of water oxidation is comparatively more challenging than the reduction of H₂ in an artificial context. Moreover, it proceeds at a rate that is five times slower than the hydrogen evolution process. The photocatalytic water splitting process encompasses several pivotal stages.[77].

1.7.1 Photon Absorption:

The initial stage of the process involves the absorption of photons emitted by a light source. Photocatalyst materials, such as α -Fe₂O₃ or CdS, have the ability to absorb photons that possess energies that are equal to or exceed their respective bandgaps. The process of absorption facilitates

the transition of electrons from the V-B to the C-B, resulting in the generation of electron-hole pairs[78].

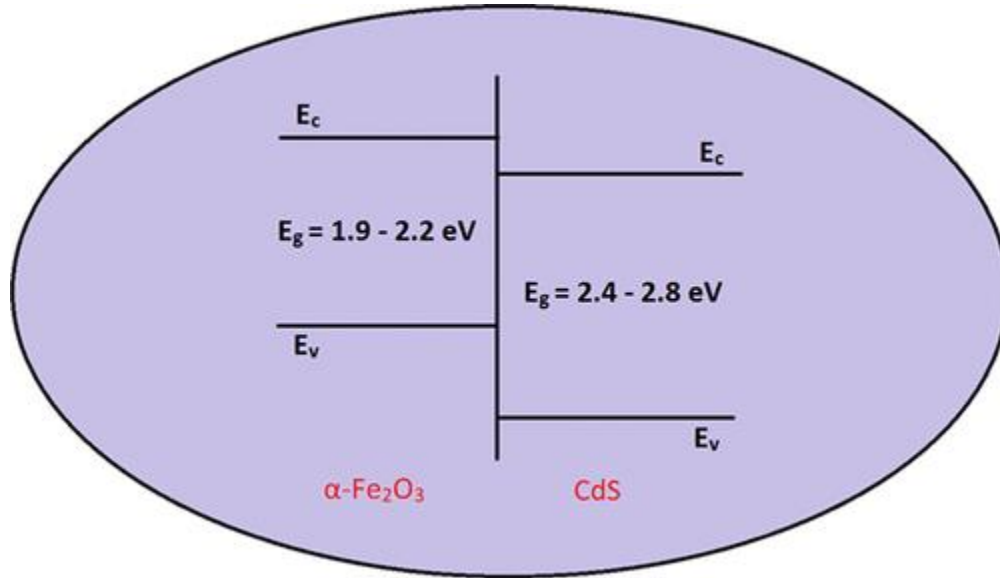


Figure 12 : Fe_2O_3 and CdS Band structure[79]

1.7.2 Photogenerated Charge Separation:

Following the absorption of photons, the electrons and holes undergo a process of charge separation. The phenomenon of separation is a result of either the inherent electric field present in the photocatalyst material or the existence of a heterojunction that exhibits appropriate energy band alignment. The electrons that have been excited by the photo migrate towards the conduction band, whereas the holes either remain in the valence band or are transferred to other materials present in the heterojunction[80].

1.7.3 Charge diffusion and transport

These are crucial processes in following charge separation in photocatalysis. Once the electrons and holes are photoexcited, it is imperative that they are effectively transported to the active sites of the catalyst. This particular step encompasses the phenomenon of charge diffusion occurring within the material of the photocatalyst, or alternatively, the transport of charges across interfaces

in the context of heterojunctions. The optimization of charge diffusion and transport is of utmost importance in order to minimize recombination events and enhance the likelihood of reaching the catalytic sites[81].

1.7.4 Catalytic Reactions surface:

Upon reaching the active sites of the catalyst, the photoexcited electrons and holes engage in reactions. In the process of water splitting, the photoexcited electrons are engaged in the removal of water molecules (H_2O) to generate H_2 , while the holes are involved in the oxidation of water molecules to liberate oxygen (O_2). The catalytic reaction takes place at distinct active sites located on the catalyst surface [82].

1.7.5 Mass Transfer:

The final phase entails the transportation of reaction byproducts, specifically hydrogen gas and oxygen gas, from the catalyst's active sites. The optimization of mass transfer is crucial in order to mitigate the accumulation of gases and facilitate the uninterrupted progression of catalytic reactions. The implementation of this procedural measure ensures the effective separation of the produced H_2 and O_2 gases, thereby facilitating their subsequent recovery for utilization as an eco-friendly and sustainable energy source[81].

Every individual step in the process plays a crucial and indispensable role in attaining optimal and environmentally friendly water splitting for the purpose of hydrogen generation. The optimization of these steps is a primary area of interest for researchers, who aim to enhance the overall performance of the system through the design of appropriate photocatalyst materials, heterojunctions, and reactor configurations.

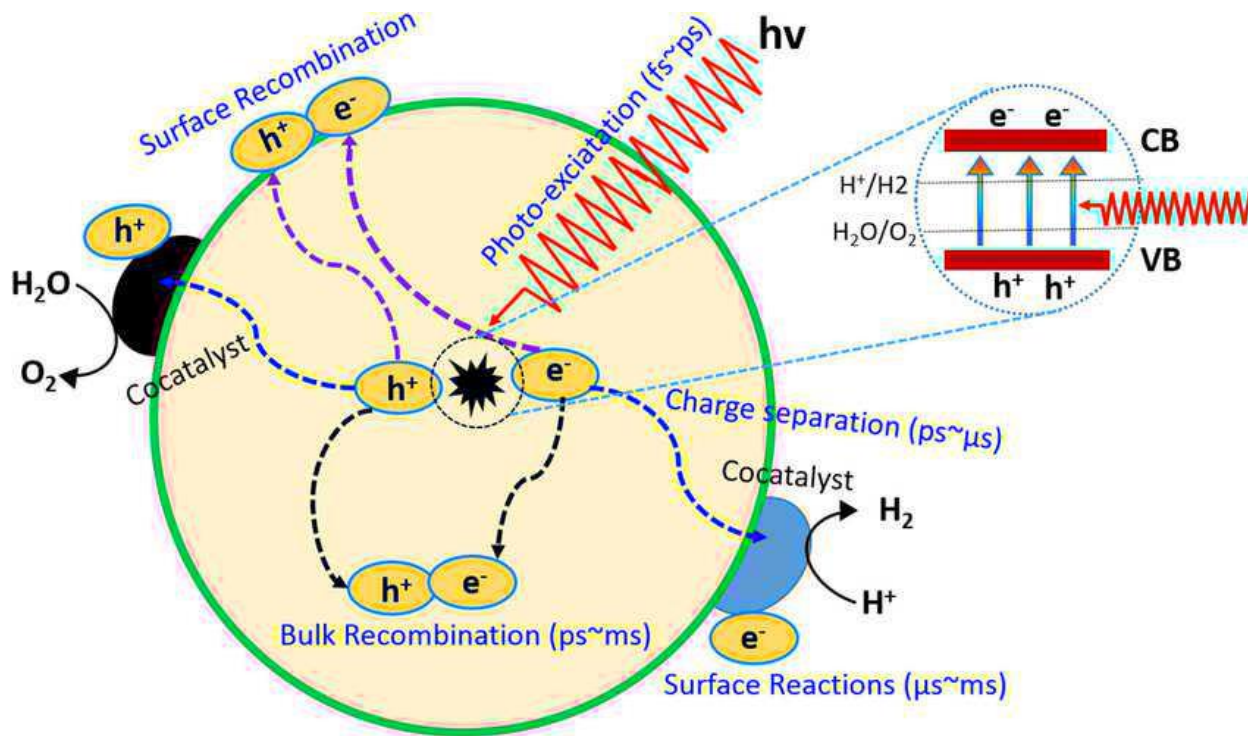


Figure 13: Mechanism of photocatalytic water splitting[83]

2 Literature Survey:

In their study, Yu et al. (2014) documented that the tetraethylenepentamine (TEPA) solvent was utilized to synthesize CdS nanowires, which demonstrated the most substantial visible-light photocatalytic H₂ production rate. This rate reached an impressive 803 $\mu\text{mol h}^{-1}$. The determined value was discovered to be roughly 2.2 times higher than the observed rate for CdS nanoparticles synthesized in dodecyl amine (DDA) solvent. The enhanced migratory properties of photogenerated electrons and holes towards the surface-active sites can be ascribed to the reduced dimensions of the nanowire structure[84].

Simon et al. utilized anion radicals to facilitate the transfer of holes from Ni/CdS to the scavenger. They achieved a rate of 64 $\text{mmol h}^{-1} \text{g}^{-1}$ and an AQE of 52.9% under laser at 447 nm. The enhanced

activity can be attributed to the rapid channeling of holes, which contributes to the of CdS and ultimately enhances the overall process of water splitting. In a separate investigation, Peng et al. synthesized Ni@C/CdS and evaluated its efficacy as a photocatalyst for the generation of H₂ from water in an aqueous solution, utilizing Na₂SO₃ and Na₂S as hole scavengers. They observed a rate of 3.23 mmol h⁻¹ g⁻¹ when employing a 320 W Xe-lamp with an irradiation intensity above 430 nm. The better execution can be ascribed to the presence of Ni deposited on the surface of CdS, which is supported by the presence of g-C acting as an electron acceptor[85].

The findings of Wang et al. imply that the inclusion of metallic cadmium significantly influences the photocatalytic activity. The hydrogen production rate through photocatalysis in pure CdS is comparatively low, as expected, due to the swift reintegration of electrons in the (CB) and holes in (VB). The observed activity of the Cd/CdS sample with a ratio (R) of 5 is found to be slightly enhanced, reaching a value of 740 μmol h⁻¹, when metallic cadmium is present. At the point where R equals 7, the average rate of H₂-production reaches its peak value of 1753 μmol h⁻¹, representing an approximate increase of 7.5 times compared to the H₂-production rate of pure CdS. Furthermore, it is worth noting that the rate of H₂ production is significantly higher compared to the majority of semiconductor photocatalysts[86].

The researchers Zeng et al. made a significant finding regarding the synthesized graphene-CdS nanocomposite. They observed that this nanocomposite demonstrated promising performance in the process of hydrogen production through photocatalysis, achieving a rate of 420 μmol h⁻¹. Furthermore, the nanocomposite exhibited an observed quantum efficiency (AEQ) of approximately 10.4% under irradiation at a wavelength of 420 nm[87].

In their study, Lang et al. conducted the synthesis of CdS–MoS₂ and CdS–MoS₂–graphene nanocomposites using a two-step solvothermal process. This method allowed for accurate

manipulation of the morphologies of CdS and MoS₂. The synthesized binary CdS-MoS₂ nanocomposite exhibits enhanced visible-light photocatalytic efficiency for hydrogen (H₂) generation in an aqueous solution containing lactic acid, when compared to both a CdS-graphene nanocomposite and a conventional platinized CdS photocatalyst. Furthermore, it is important to highlight that the ternary CdS-MoS₂-graphene nanocomposite exhibits the highest degree of activity in relation to the production of H₂ through visible-light photocatalysis. This is evidenced by a rate of 621.3 $\mu\text{mol h}^{-1}$ and an apparent quantum efficiency of 54.4 % at a wavelength of 420 nm [88].

The determination of the (AQE) for hydrogen (H₂) production was led under identical photocatalytic reaction states, except for the utilization of a 30 W 420 nm-LED lamp as the source of monochromatic light. The measured area of irradiation was determined to be 4 cm², while the average intensity of light irradiation was recorded as 30.5 mW/cm². Upon exposure to the aforementioned light irradiation, the catalyst 2.0 wt % Pt/CdS/ Fe₂O₃⁻³ exhibited H₂ production rates of 158.04 $\mu\text{mol h}^{-1}$ and 252.86 $\mu\text{mol h}^{-1}$ in benzylamine substrate solutions with concentrations of 3 mmol and 10 mmol, respectively[82].

The evaluation of the photocatalytic performance of composites comprising ZnO, Fe₂O₃, and g-C₃N₄ was conducted by N. Mao et al. This evaluation involved assessing the production of H₂ through the process of water splitting. The experimental results suggest that the ZnO/Fe₂O₃/g-C₃N₄ composite demonstrates improved hydrogen (H₂) production efficiency in comparison to pure g-C₃N₄ under visible-light irradiation. The rate of hydrogen (H₂) production was determined to be 25 $\mu\text{mol}\cdot\text{h}^{-1}$ using the 3-ZnO/ Fe₂O₃/g-C₃N₄ composite. The observed rate of H₂ production when using a combination of g-C₃N₄ and another substance is four times higher than the rate observed when using pure g-C₃N₄ alone. The findings of this study indicate a significant

improvement in the photocatalytic performance of the nanocomposite material that was synthesized[89].

The deficiency of photocatalysts exhibiting both high efficiency and stability upon activation by solar light has been a major obstacle in the advancement of this technology, as investigated by G. Carraro et al. This study aims to conduct an examination of two iron (III) oxide polymorphs, specifically β - Fe_2O_3 and ε - Fe_2O_3 , which have been subject to limited investigation in prior scholarly studies. The observed polymorphs demonstrate a remarkable ability to produce hydrogen (H_2) when exposed to sunlight in the presence of aqueous solutions containing sustainable oxygenates like ethanol, glycerol, and glucose. The hydrogen production rates for β - Fe_2O_3 and ε - Fe_2O_3 are observed to reach maximum values respectively. These findings indicate a notable enhancement in performance when compared to the extensively investigated α - Fe_2O_3 [90].

Yujie Li, Lei Ding et-al contributed that while photocatalytic activity of pure TiO_2 nanosheets (NSs) is observed, however, the rate of hydrogen (H_2) evolution is relatively low, measuring at $54.3 \mu\text{mol g}^{-1} \text{h}^{-1}$. This can be attributed to the rapid recombination of electrons and holes. As anticipated, the rate of photocatalytic hydrogen (H_2) evolution for the $\text{MoS}_2@\text{TiO}_2@\text{Ti}_3\text{C}_2$ composites at a temperature of 180°C exhibits a substantial enhancement, measuring at $2128.3 \mu\text{mol g}^{-1} \text{h}^{-1}$. This value is nearly 39 times higher than that of pure TiO_2 nanosheets (NSs). The utilization of the Ti_3C_2 MXene and MoS_2 as co-catalysts is essential for effectively capturing photo-generated electrons, a critical factor in enhancing the photocatalytic activity of the heterostructure for H_2 production. Significantly enhanced photocatalytic performance is observed following the introduction of molybdenum vacancies. The $\text{Mo}_x\text{S}@\text{TiO}_2@\text{Ti}_3\text{C}_2$ composites (160°C) exhibit the highest photocatalytic H_2 evolution rate of $10505.8 \mu\text{mol g}^{-1} \text{h}^{-1}$, which is

approximately 193 and 6 times greater than the rates observed for pure TiO₂ NSs and MoS₂@TiO₂@Ti₃C₂ composites (160 °C), respectively[91].

In their study, Yin et al. (2020) successfully synthesized a ternary nanocomposite, denoted as MXene@Au@CdS, which exhibits promising characteristics for utilization in the realm of capable and high-performance photocatalytic hydrogen production. The composite material consisting of MXene@Au@CdS demonstrates a H₂ rate of 17.07 mmol h⁻¹g⁻¹ during a 2-hour testing duration. The observed rate for this particular material is 1.85 times greater than the rate observed for pure CdS nanomaterials. The increased efficiency of hydrogen production in the MXene@Au@CdS composite can be ascribed to two primary factors. The inclusion of MXene enhances the availability of active adsorption sites and reaction centers for the Au and CdS nanoparticles. This mechanism enhances the synergy among various constituents and fosters optimal hydrogen generation. Furthermore, the robust surface plasmon resonance displayed by gold (Au) has a mutually beneficial impact on the optical response spectrum of cadmium sulfide (CdS), resulting in an extended range of wavelengths that can be absorbed and harnessed for the purpose of hydrogen production[92].

The authors, Yuying Wang et al., provided an explanation regarding the application of a composite system that combines 2D Ti₃C₂ MXene and 3D CdS nanoflowers. This composite system has been observed to effectively enhance the transfer and separation of carriers, resulting in improved performance of CdS. In comparison to pure CdS nanoflowers, the Ti₃C₂@CdS composite demonstrates a decrease in photoluminescence intensity, an extension of fluorescence lifetime, an increase in photocurrent density, and a decrease in electrochemical impedance. The photocatalytic activity for hydrogen evolution is significantly enhanced in the composite material composed of Ti₃C₂@CdS, wherein the titanium carbide (Ti₃C₂) content is 15 wt%. The measured rate of

hydrogen evolution is recorded as $88.162 \mu\text{mol g}^{-1} \text{h}^{-1}$, exhibiting an approximate increase of 91.57 times compared to the rate observed for pure CdS [93].

3 Synthesis:

3.1 Synthesis of 2D CdS:

CdS nanosheets were synthesized by using standard solvothermal method. Cadmium acetate Dihydrate [$\text{Cd}(\text{Ac})_2 \cdot 2\text{H}_2\text{O}$], thiourea [$\text{SC}(\text{NH}_2)_2$] were used as precursor for the preparation of CdS nanosheets. 2mmol of cadmium acetate and 6mmol of thiourea were dissolved in 60ml of Ethylene diamine and stirred for 10 mins. The reaction was carried out in 100ml Teflon- lined stainless-steel autoclave at 105°C for 8h. After the reaction was finished, autoclave was cooled to room temperature. Centrifugation at 8000rpm for 10 minutes resulted in the collection of solid products. It was repeatedly cleaned in ethanol and distilled water before being dried in a vacuum oven at 60°c . So pale yellow CdS powder was extracted.

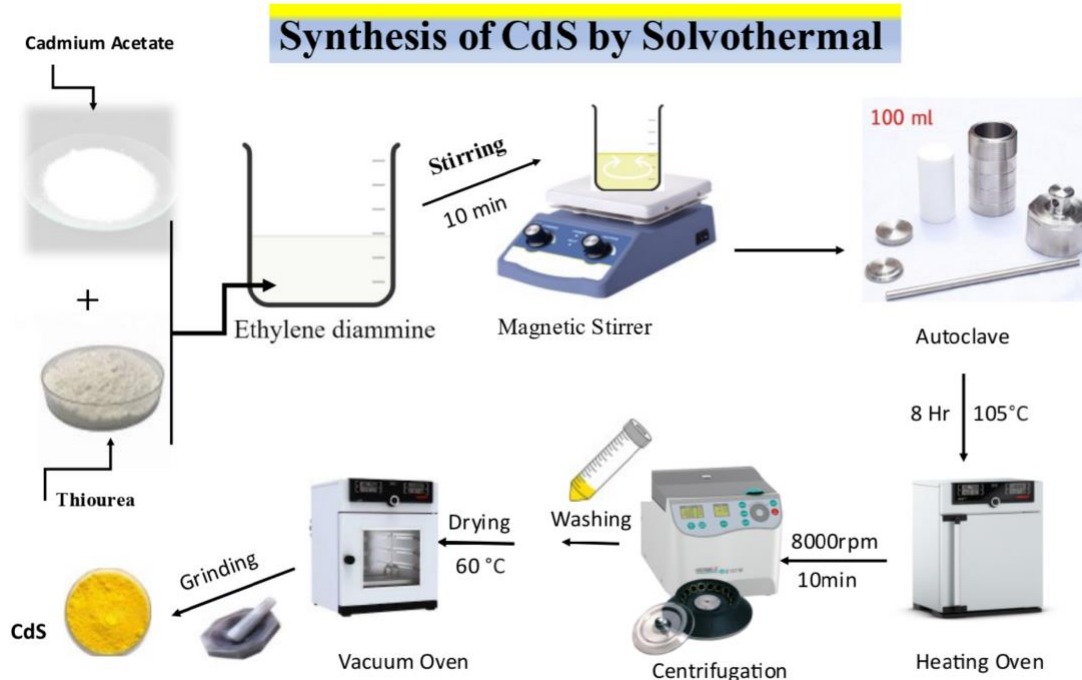


Figure 14: Synthesis of 2D CdS

3.2 Synthesis of Fe₂O₃ Nanosheets:

A common method for synthesizing α -Fe₂O₃ nanosheets involved dissolving 1 mmol of iron chloride hexahydrate [FeCl₃·6H₂O] and 0.25 mmol of aluminum sulfate [Al₂(SO₄)₃] in 10 ml deionized water with magnetic stirring. Light brown solution was given a dropwise addition of 3ml triethylamine which was then stirred for another 20 minutes. After that, this mixture was made into a 50 ml Teflon-lined stainless-steel autoclave, sealed and heated at 160°C for 24 h. As soon as reaction was completed autoclave was left to cool down on its own. After the hydrothermal treatment the liquid was allowed to separate from the solid product by centrifugation. Centrifugation at 8000rpm for 20 minutes was used to gather the red precipitates. After being cleaned the red product was dried in vacuum oven at 60°C.

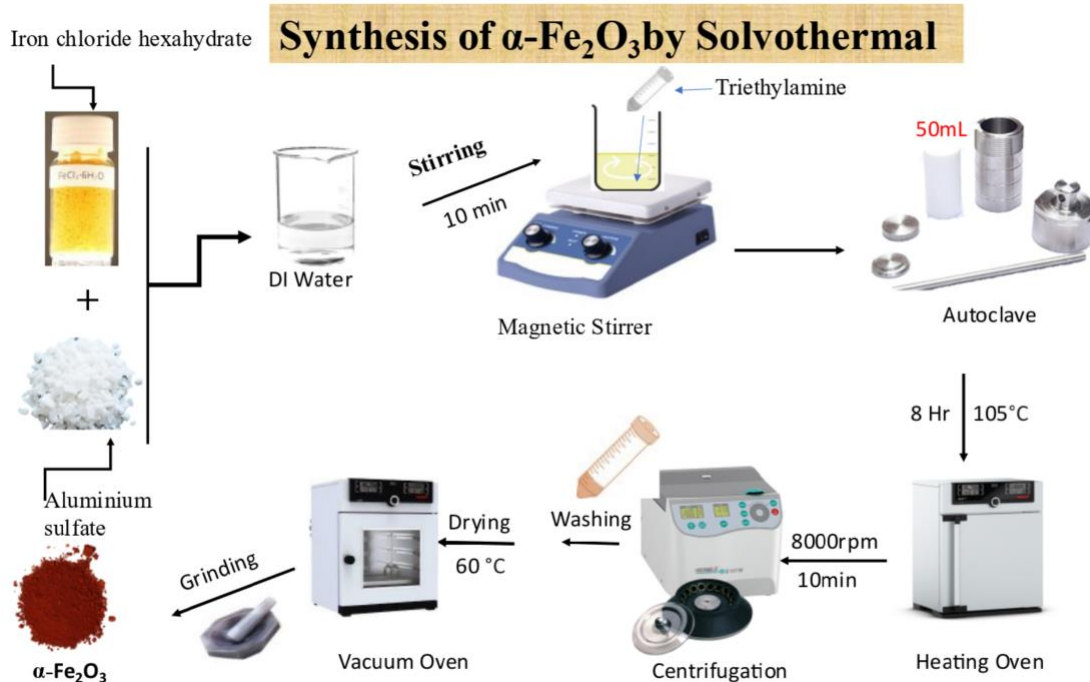


Figure 15: Synthesis of Fe₂O₃ BY SOLVOTHERMAL METHOD

3.3 Synthesis of Nickel nanoparticles:

Synthesis of nickel nanoparticles was performed by using reflux set up. The chemical precursors used in the synthesis of nickel nanoparticles were nickel nitrate hexahydrate [Ni (NO₃)₂.6 H₂O], Polyvinylpyrrolidone PVP, Sodium hydroxide (NaOH) and hydrazine monohydrate [N₂H₄.H₂O]. In this reaction, 0.872g of Nickel nitrate hexahydrate was dissolved in 100 ml of Ethylene glycol then 1g of PVP was added in the solution. A clear green solution was turned blue by addition of 3 ml of hydrazine monohydrate. After the addition of 0.8 g of sodium hydroxide pellets the solution was poured into 250 ml of round bottom flask and condenser is attached at the top. A stir bar was added in the round bottom flask and temperature was maintained 80⁰C for 12 h. As soon as the sodium hydroxide pellets were dissolved the solution turned black. After the completion of reaction black precipitates were separated from liquid phase. The solid product was washed thrice

with ethanol to remove contaminants. After washing with ethanol, the product was dried in vacuum oven at 60°C for 5h.

3.4 Synthesis of Mxene:

1.6g of LiF powder was gradually added into 22mL of 9.1 M HCl solution. It was magnetically agitated for approximately 20 minutes until opaque solution changed into clear solution. Then, 1 g of MAX powder (Ti_3AlC_x) was gradually dissolved into the etching solution mentioned above while being constantly stirred, and was then stirred for the following 24 hours at RT. The obtained solution was washed several times with Deionized water by centrifugation at 8000rpm and the time for each cycle was kept 10 minutes until the pH of the solution become neutral. Final homogeneous dark green product was collected by centrifugation at 3500rpm for 1h. Final product obtained was 20-30mg/ml.

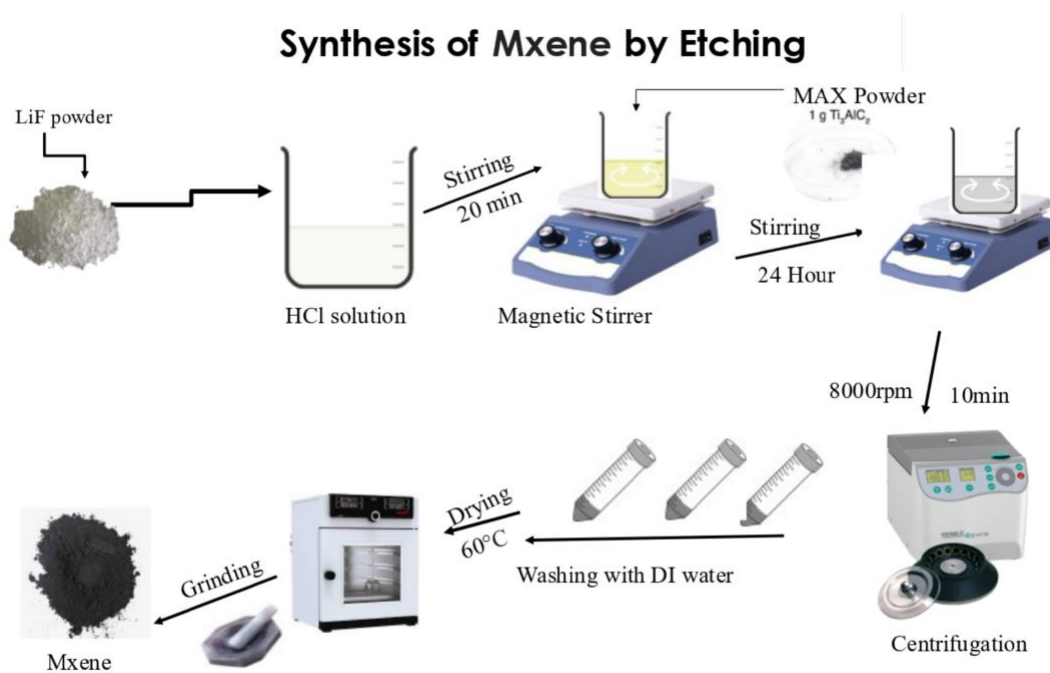


Figure 16 :Synthesis of Mxene by etching

3.5 Formation of α -Fe₂O₃ /CdS Heterojunctions:

Synthesis of α -Fe₂O₃ /CdS heterojunction involves the following steps:

First precursor solution of CdS was prepared and shifted to Teflon lined stainless steel autoclave. Then α -Fe₂O₃ was added in the above solution in different ratios (5%, 15%, 25%, 35%, 45% etc.). After the addition of α -Fe₂O₃ heterojunction is developed between CdS and α -Fe₂O₃. Then autoclave was placed in oven at 105⁰C for 8h. Orange brown precipitates of α -Fe₂O₃/CdS were collected after centrifugation and dried in vacuum oven at 70⁰C.

3.6 Synthesis of α -Fe₂O₃/Mxene /CdS:

Synthesis of ternary heterojunction was performed by solvothermal treatment. Different ratios of α -Fe₂O₃ (25%, 35% etc.) and Mxene (7%, 12%) were added in 60 ml of Ethylene diamine and sonicated for 30 minutes. Then the precursors of CdS were added in the above solution. Stir bar was added and solution was stirred for 20 minutes. Solution was transferred in Teflon lined stainless steel autoclave and placed in oven at 105⁰C for 8h. Solid product was washed and dried in oven at 60⁰C for 6h. For better performance of catalyst these parameters should be considered i.e., ratio of α -Fe₂O₃ and Mxene to CdS, morphology of composite and synthesis conditions.

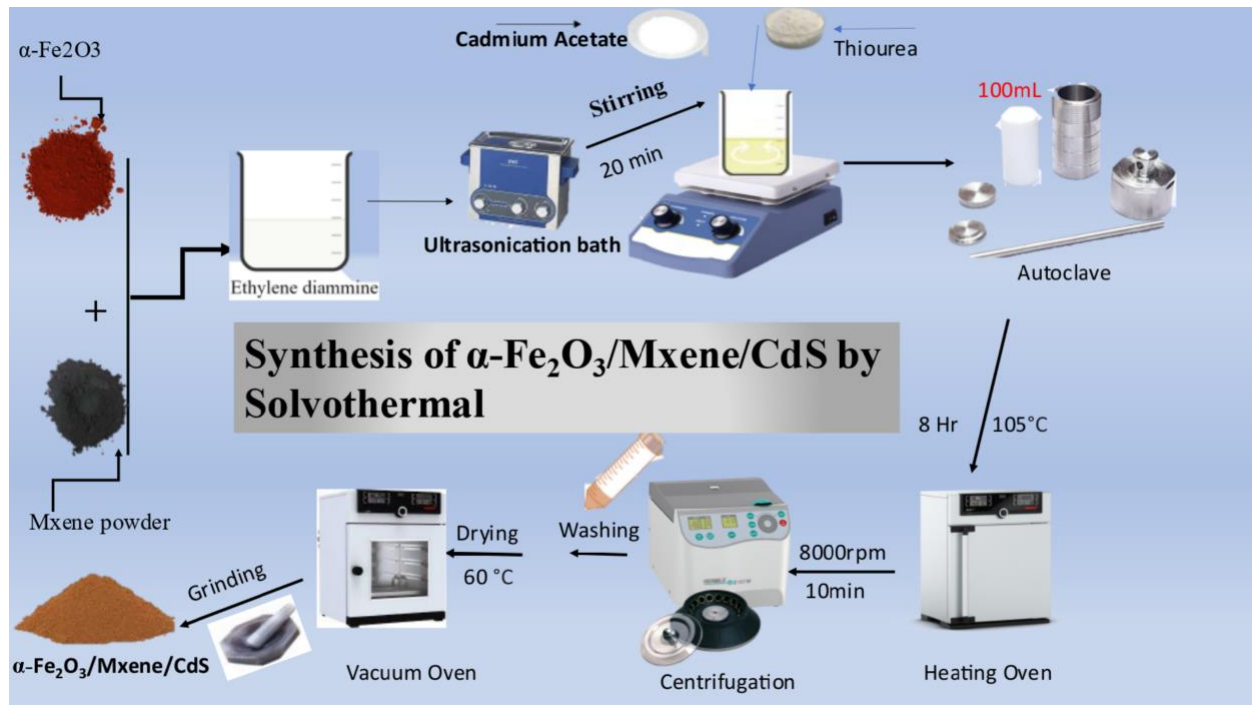


Figure 17 :Fabrication of Ternary Heterojunction

4 Characterization:

4.1 XRD:

4.1.1 XRD of CdS/ α -Fe₂O₃:

Crystal structure can be determined by performing XRD analysis. The six CdS diffraction peaks can be attributed, according to the XRD patterns, to the hexagonal wurtzite crystal planes (100), (002), (101), (102), (110), (103), and (112). The two thetas of 24.8°, 26.5°, 28.2°, 36.6°, 43.7°, 47.8° and 51.8° correspond to these peaks.

Based on the provided information, it can be concluded that the observed X-ray diffraction (XRD) pattern corresponds to the characteristic pattern of hematite (α -Fe₂O₃) as indicated by ICDD card no. 33-0664. The lattice constants of the rhombohedral (hexagonal) structure of α -Fe₂O₃ are

reported to be $a = 0.5034$ nm and $c = 1.375$ nm. This means that the unit cell of hematite has a rhombohedral shape with these specific dimensions. The peaks observed at specific 2θ angles, namely 24.16° , 33.12° , 35.63° , 40.64° , 49.47° , 54.08° , and 57.42° , can be assigned to specific crystalline structures within the $\alpha\text{-Fe}_2\text{O}_3$ nanoparticles. Specifically, these peaks correspond to the (012), (104), (110), (113), (024), (116), and (018) crystallographic planes of hematite. The narrow and sharp peaks in the XRD pattern indicate that the hematite nanosheets are highly crystalline. This suggests that the synthesized hematite particles have a high level of purity, which is achieved through the described synthesis method. Additionally, the information suggests that increasing the precursor concentration of $\text{FeCl}_3 \cdot 6\text{H}_2\text{O}$ leads to certain changes in the XRD pattern. Specifically, the intensity of the (104) diffraction peak gradually decreases, and its half height width is reduced. These changes in the peak characteristics indicate an increase in particle size as the precursor concentration increases.

4.1.2 XRD of MAX and Mxene :

The XRD pattern of MAX shows (002), (104), (105), (110), and (118) crystal planes that are represented by the five distinct peaks that emerged at 9.52° , 39.04° , 41.82° , 60.26° , and 74.11° . The (002) peak of Ti_3AlC_2 , which is initially at 9.5° , is clearly widened and displaced to a lower angle (7.53°) after exfoliation with LiF and HCl. Mxene is the owner of this peak. The most prominent diffraction peak at 39.04° nearly vanished, indicating a shift from Ti_3AlC_2 to Ti_3C_2 Mxene in the crystal structure. A good LiF and HCl etching action is shown by the elimination of the preferred orientation along the (104) plane and the shifting of the (002) peak of Ti_3AlC_2 . According to calculations, the lattice parameter c of Ti_3AlC_2 is 18.6 while that of $\text{as-Ti}_3\text{C}_2\text{T}_x$ is 23.4. The rise in the c -lattice parameter, which is related to the layered structure of Mxene, may be the cause of this shift. These modifications attest to the Mxene flakes' effective production. A minor amount of TiO_2

was created during the MAX phase etching procedure and could be seen in the XRD pattern in the range 40–45°.

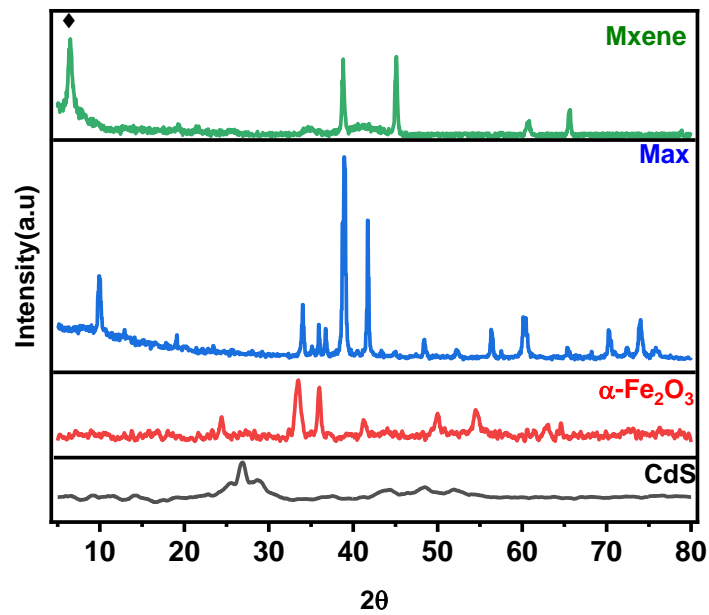


Figure 18: Xrd of CdS, α -Fe₂O₃, Max and Mxene

4.1.3 XRD of binary and ternary heterojunction:

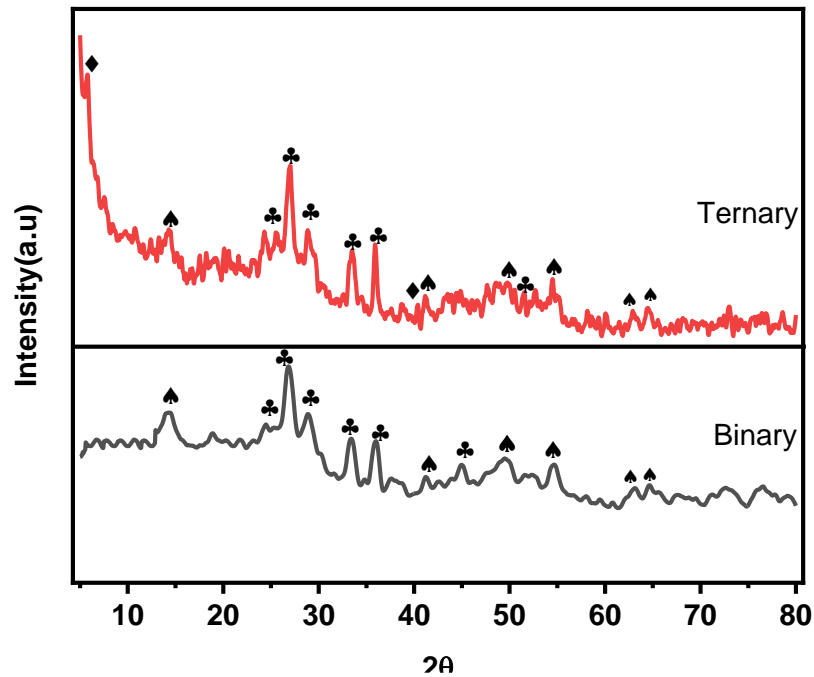


Figure 19: XRD of Binary and Ternary heterojunctions

In XRD pattern of CdS/Fe₂O₃ black flower shows CdS which is well matched with XRD pattern of CdS (JCPDS-41-1049) While black heart indicates α -Fe₂O₃ which matches well with XRD pattern of α -Fe₂O₃ (JCPDS-03-0664).

4.2 X-ray Photoelectron Spectroscopy:

A potent tool for determining the chemical make-up and element valence of the α -Fe₂O₃/CdS composite is the X-ray photoelectron spectroscopy (XPS) investigation. XPS survey spectrum corresponds to the signals of Ti2p, C1s, Fe2p, O1s, Cd3d, S2p. XPS spectrum of Fe2p exhibited two peaks at 710.4 and 724.2 eV corresponds to Fe2p_{3/2} and Fe2p_{1/2} while satellite peaks are present at 719.2 and 732.9 eV. O1s shows three peaks at binding energy of 530, 531 and 532 eV making Fe-O, Fe-O-C, Fe-OH bonds.

Ti2p_{1/2}, Ti2p_{3/2} exhibit peaks at 459.1 and 457.8 eV after deconvolution doublet appear which confirm the formation of ternary composite by showing the bond between titanium and carbon, titanium and oxygen. C1s spectra shows C-C bond and C-O bond at binding energy of 284.8 and 287 Ev.

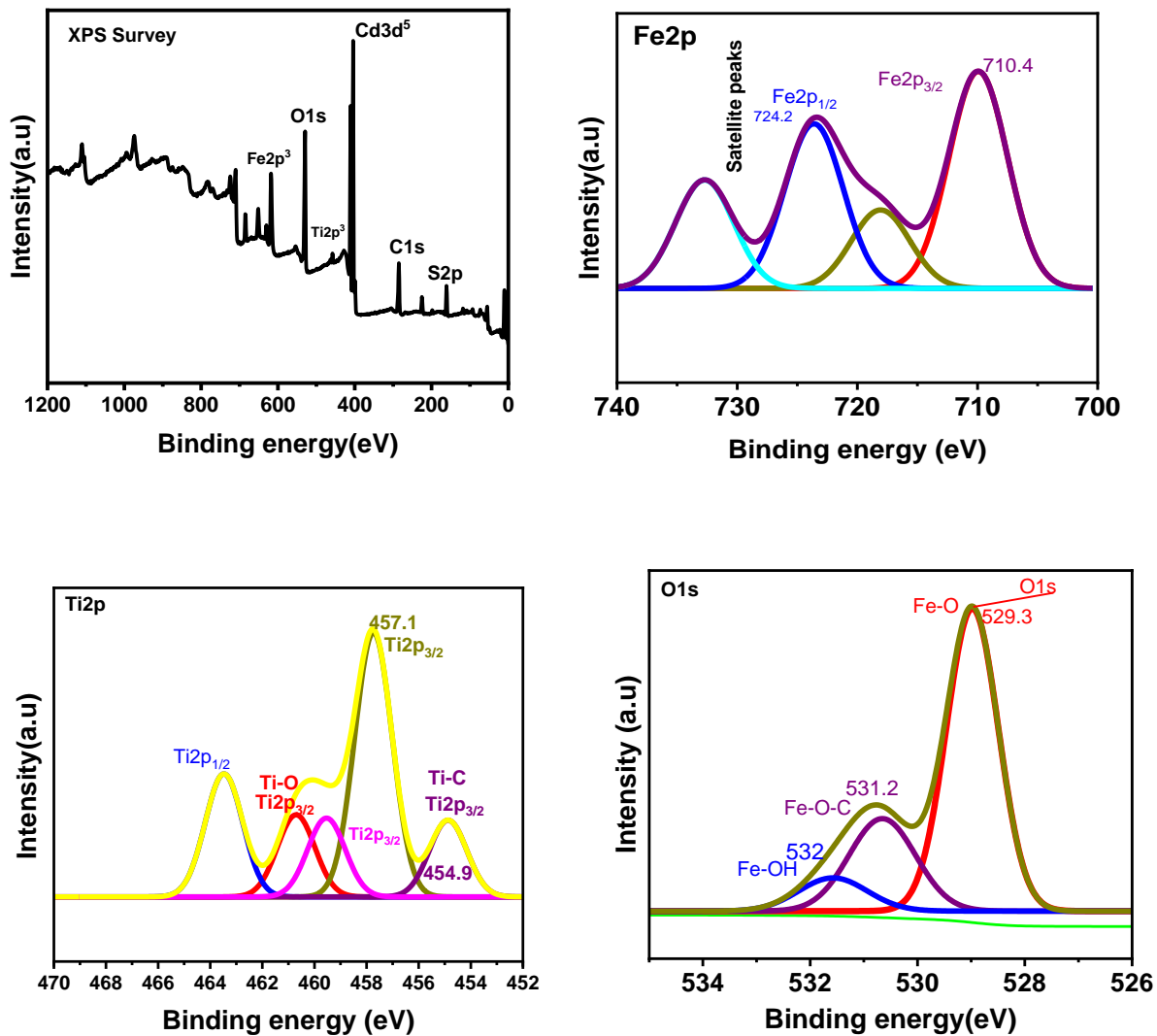


Figure 20 : a) XPS survey b) Fe2p c) Ti2p d) O1s

The α -Fe₂O₃ /CdS composite's Cd3d XPS spectrum exhibited two distinct peaks that were associated with Cd atoms in Cd-S bonds and had binding energies of 404.63 and 411.3 eV. This information shows that CdS is present in the substance, which has significant effects on its optical and electrical properties.

The S2p spectra was split into two distinct peaks, the first of which was attributed to S species from CdS with binding energy of 161.5 and 162.3 eV correspond to the S2p_{3/2} and S2p_{1/2}. This knowledge gives a thorough understanding of the material's sulfur component, which is essential for comprehending its chemical and physical behavior. In conclusion, the XPS analysis of the Mxene/ α -Fe₂O₃/CdS composite provides valuable information about its chemical composition and element valence, including the presence of various carbon, titanium, iron, oxygen sulfur, and cadmium species. This information can be used to guide future studies and applications of the material, including the optimization of its properties and performance.

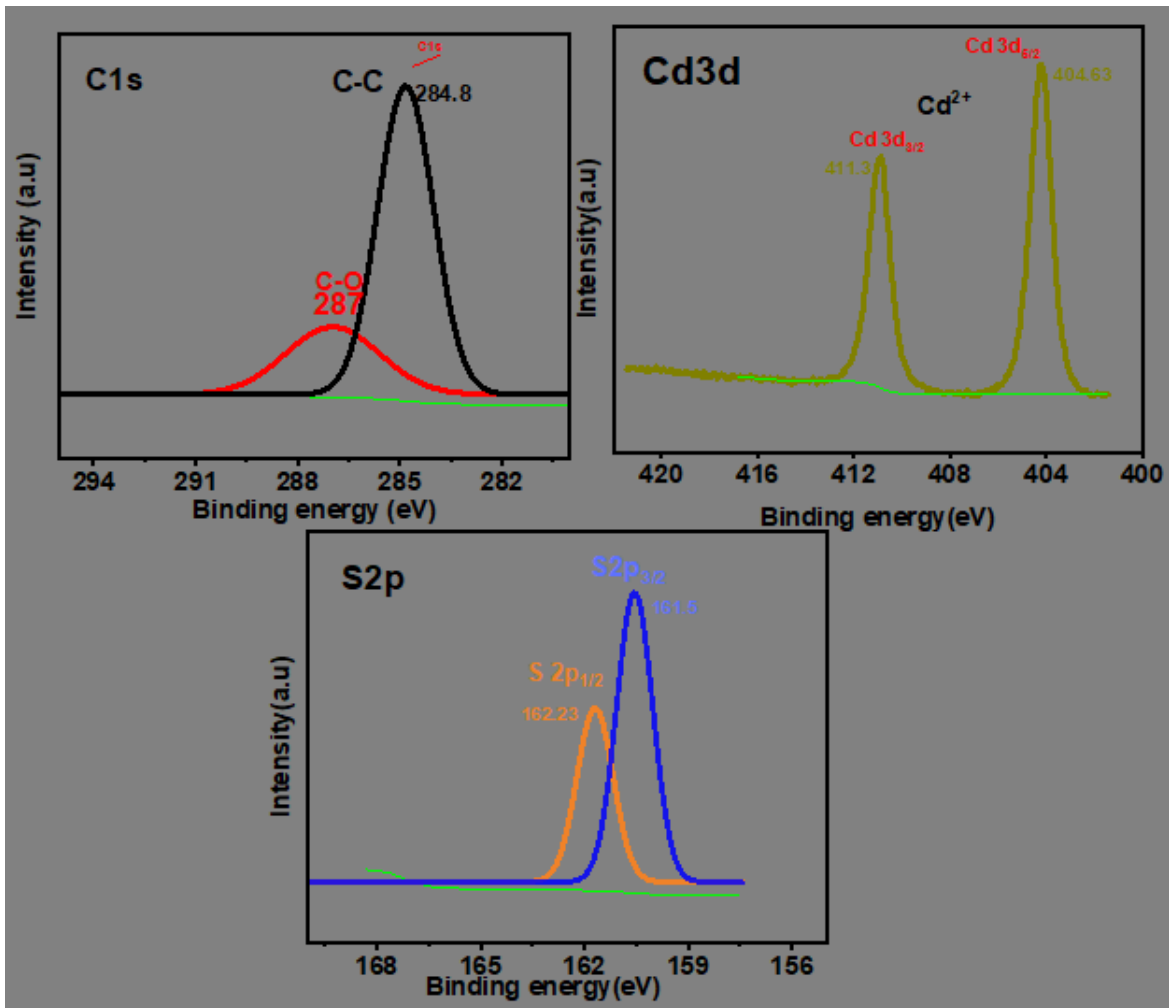


Figure 21: XPS of e) C1s f) Cd3d g) S2p

4.3 Scanning Electron Microscopy:

The semiconducting materials cadmium sulfide (CdS) and α -Fe₂O₃ have different morphologies. Due to its crystal lattice's extremely flexible and thin sheets, CdS is known to generate 2D flower-like formations. The hexagonal wurtzite crystal structure of CdS, which causes the creation of thin, flexible sheets along specific crystallographic planes, is related to the formation of such structures. α -Fe₂O₃'s flexible and ultrathin sheet-like structure is plainly visible. Rhombohedral structure of α -Fe₂O₃ causes the formation of 2D ultrathin sheets.

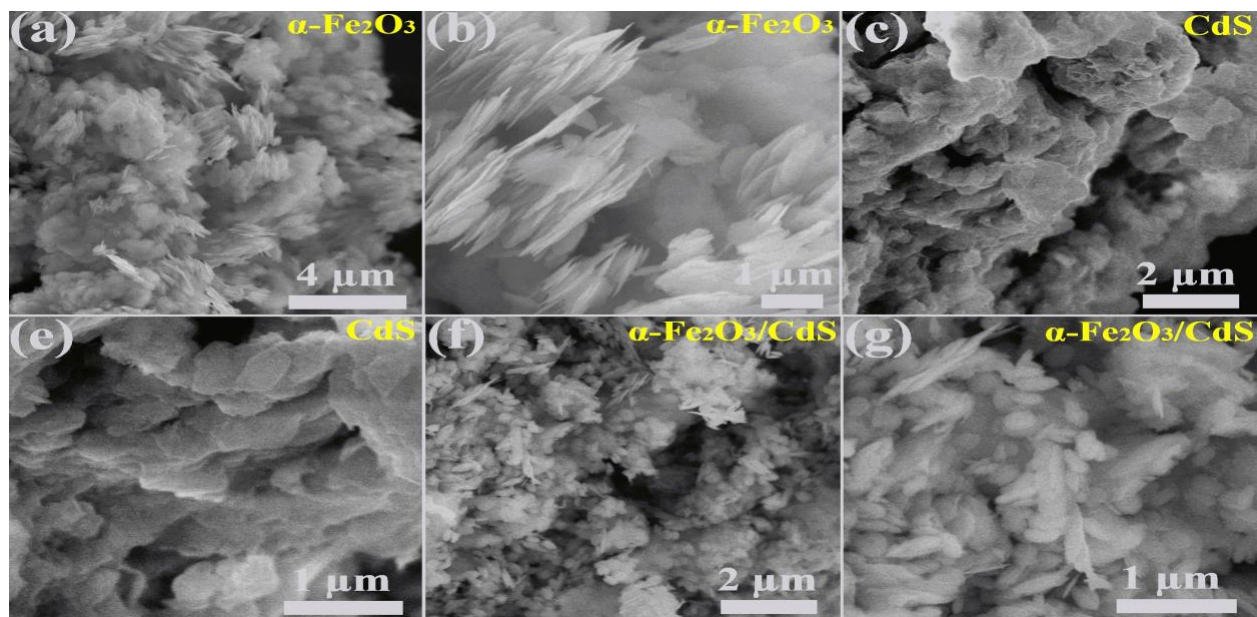


Figure 22: SEM images of a-b) α -Fe₂O₃ , c-e) CdS , f-g) α -Fe₂O₃ /CdS

Both of these materials' physical and chemical characteristics, such as surface area, electronic structure, and catalytic activity, can be influenced by their shape. Designing and maximizing these materials' applicability in a variety of sectors, such as photocatalysis and energy conversion, therefore requires an understanding of their morphology.

4.4 Transmission Electron Microscopy:

The strong and distinctive method of transmission electron microscopy (TEM) is used to characterize structures. The most significant use of TEM is for the real-time, atomic-resolution imaging of nanoparticles. TEM of Mxene shows sheet-like structure with inter-spacing of 0.98nm at (002) plane.

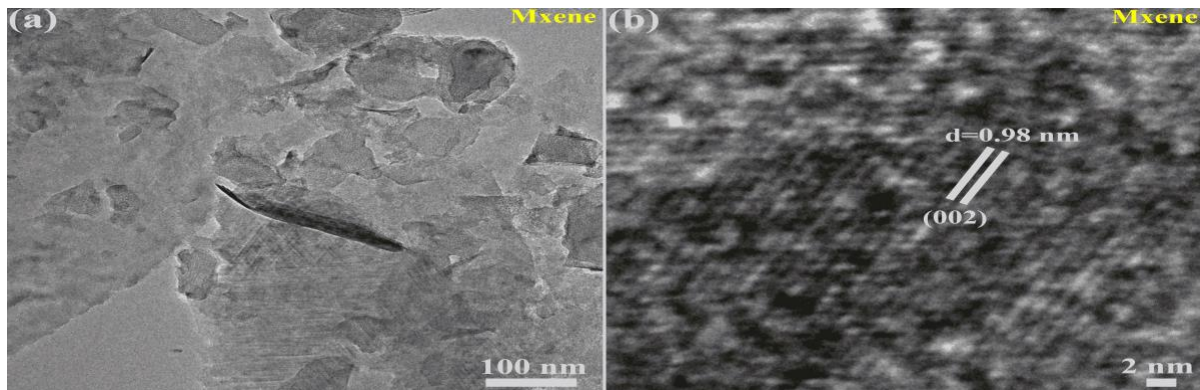


Figure 23: TEM images of Mxene

4.5 Elemental Mapping:

This is another characterization technique by which the atomic composition of my composite was confirmed as shown below; in which there is clearly seen that the formation of CdS and α -Fe₂O₃ are successfully formed via hydrothermal.

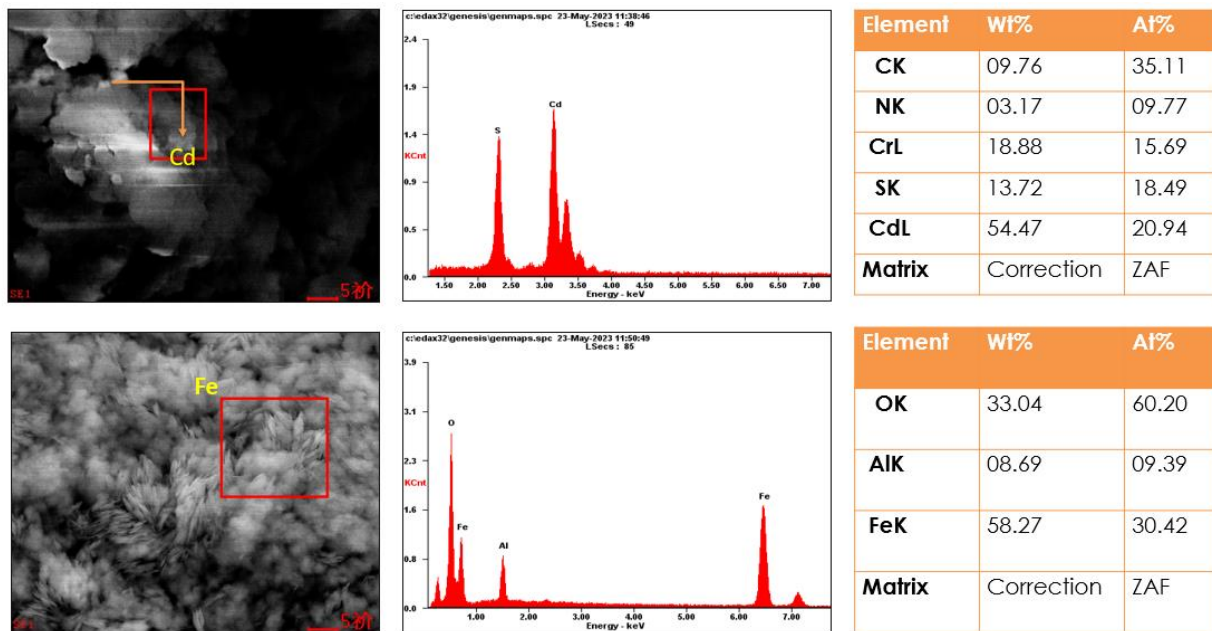


Figure 24: EDS spectra of CdS and α -Fe₂O₃

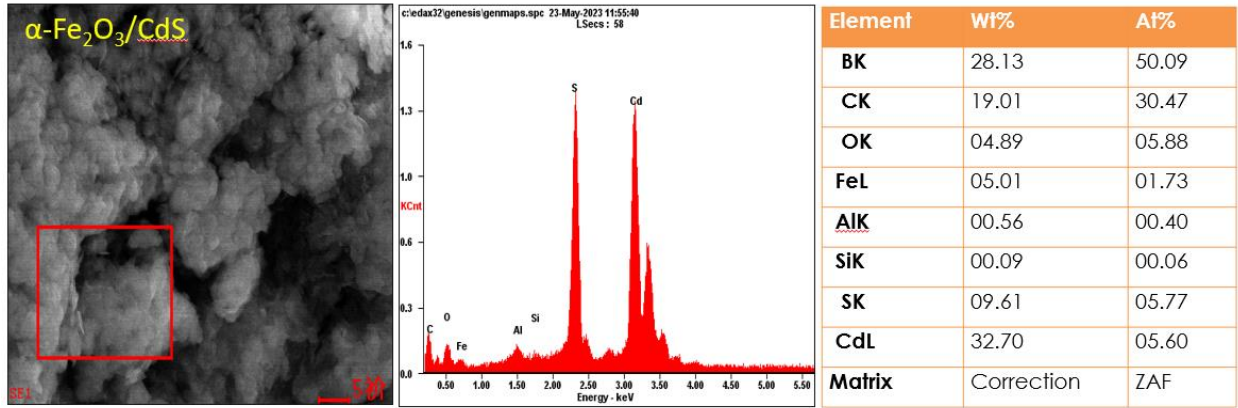


Figure 25: EDS spectra of Binary composite

4.6 UV- visible spectroscopy

UV- visible spectroscopy is a method for examining a material's electrical characteristics. UV- visible analysis can be used to determine the band gap of Mxene, $\alpha\text{-Fe}_2\text{O}_3$ and CdS composite material. The curve generated by graphing $(\alpha h\nu)^2$ versus Energy is extrapolated using a tauc plot. This makes it possible to calculate the composite material's band gap.

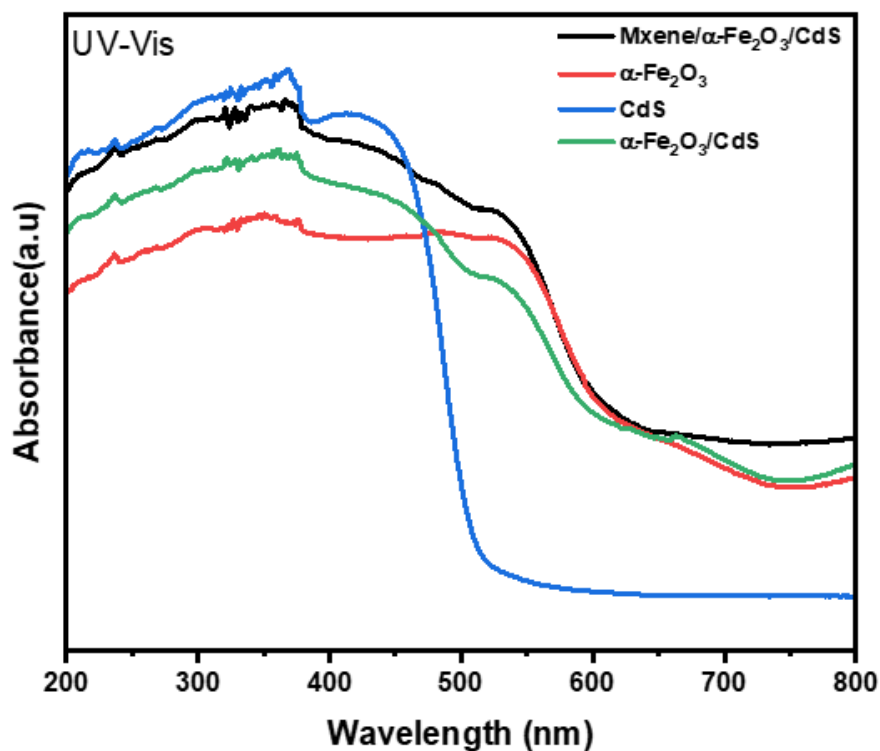


Figure 26: UV-Vis Spectroscopy

The calculated band gap values i.e., 2.42 eV, 1.94 eV, 1.85 eV, 1.76 eV for CdS, α -Fe₂O₃, α -Fe₂O₃/CdS and Mxene/ α -Fe₂O₃/CdS. This reduction in band gap suggests that the composite material will be better able to use visible light, which is advantageous for prospective uses in photocatalysis or solar cells. The technique employed for the investigation has a solid foundation in the academic literature and is frequently applied to find band gaps in a variety of materials.

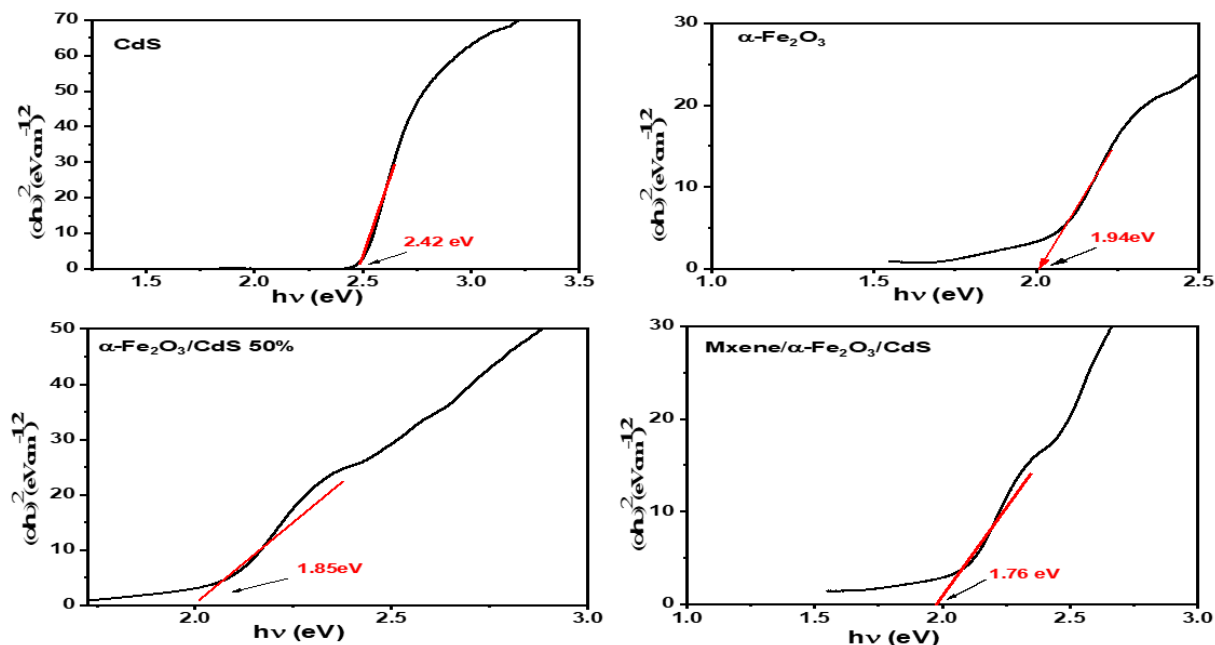


Figure 27: Band-Gaps from Tauc plots

4.7 Photoluminescence Spectroscopy:

To investigate the charge transport and separation effectiveness of Mxene/ α -Fe₂O₃/CdS heterojunctions in this situation, photoluminescence spectroscopy (PL) is a potent tool. To examine the light emission from the material, a 470nm excitation wavelength was used in the PL investigation. Information on the process of charge recombination in the material can be gleaned from the intensity of the PL spectra.

According to the findings, CdS, which has a somewhat highest intensity peak indicating the highest charges recombination rate, is followed by Mxene and α -Fe₂O₃. The α -Fe₂O₃/CdS composite exhibits lower intensity peak, which shows that there is less charge recombination there than in the original material. Electron hole recombination is further reduced by making ternary heterojunction Mxene/ α -Fe₂O₃/CdS. The presence of trap centres, flaws at the grain boundaries,

band structure, and carrier mobility in the composite material are some of the causes of this decrease in emission intensity.

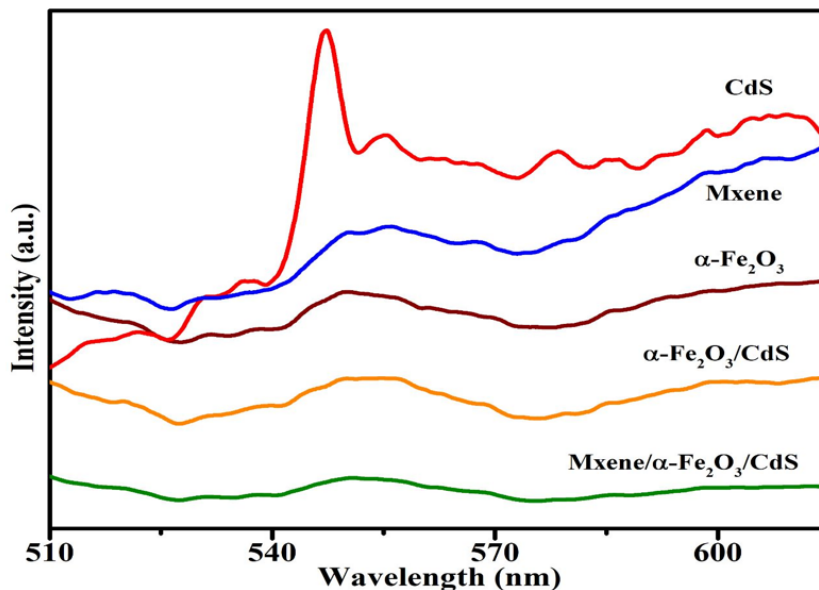


Figure 28: PL spectra

5 Applications

5.1 Photocatalytic hydrogen generation:

Photocatalytic water splitting process was executed in 100ml one side flat round bottom flask by using Xenon lamp of 300W. More specifically, 80 mL of aqueous solution containing 20 ml ethanol and 10ml of 1 M solution of NaOH were added to 10 mg of the catalyst as-prepared. This solution was sonicated for 30 minutes. The other gas was then removed from one side flat round bottom flask by evacuation with N₂ for 10 minutes. Flask was sealed tightly with rubber septum. The reactor was placed under Xenon lamp for continuous illumination for 1 h with cutoff filter of 420nm. Detection of hydrogen was done by using GC- chromatogram.

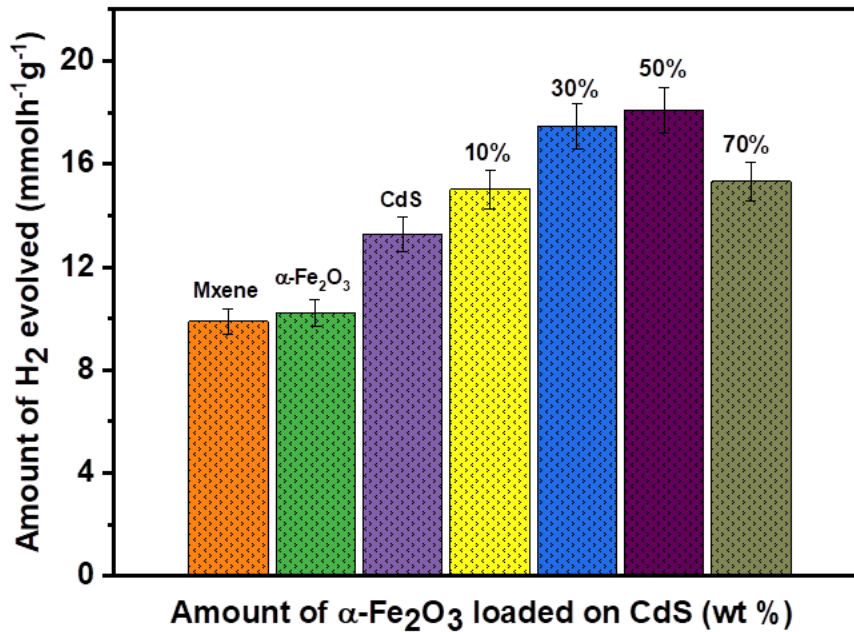


Figure 29: H_2 Evolution rate of different binary heterojunction ratio

$\alpha\text{-Fe}_2\text{O}_3/\text{CdS}$ demonstrated a greater efficiency for hydrogen generation than bare CdS and $\alpha\text{-Fe}_2\text{O}_3$. We have seen that the stability of CdS is enhanced when $\alpha\text{-Fe}_2\text{O}_3$ and cocatalysts are used. The hydrogen production activities of the catalysts $\alpha\text{-Fe}_2\text{O}_3(10)/\text{CdS}(90)$, $\alpha\text{-Fe}_2\text{O}_3(30)/\text{CdS}(70)$, $\alpha\text{-Fe}_2\text{O}_3(50)/\text{CdS}(50)$, $\alpha\text{-Fe}_2\text{O}_3(70)/\text{CdS}(30)$ were $15.02 \text{ mmol g}^{-1} \text{ h}^{-1}$, $17.44 \text{ mmol g}^{-1} \text{ h}^{-1}$, $18.08 \text{ mmol g}^{-1} \text{ h}^{-1}$ and $15.31 \text{ mmol g}^{-1} \text{ h}^{-1}$ respectively.

5.2 H_2 Production of Mxene/ $\alpha\text{-Fe}_2\text{O}_3/\text{CdS}$:

The most effective catalysts were discovered to be the composites (Mxene/ $\alpha\text{-Fe}_2\text{O}_3/\text{CdS}$) that were manufactured with an overall 12% loading of mxene on CdS. The H_2 production activity was $51.04 \text{ mmol g}^{-1} \text{ h}^{-1}$ respectively.

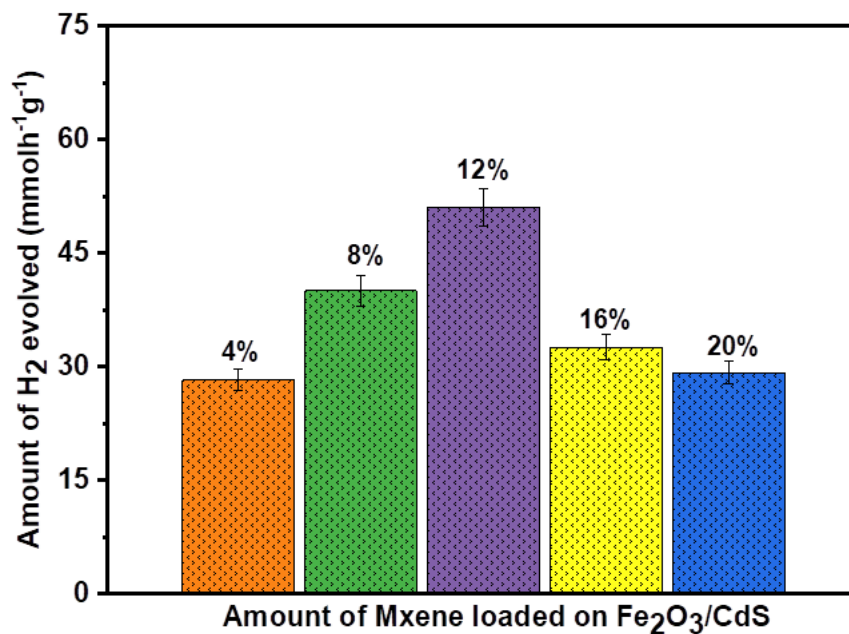


Figure 30: H₂ evolution rates of different concentration of Mxene loaded

5.3 H₂ Production of ternary heterojunction with Different Sacrificial reagents:

It could be clearly seen that H₂ Production was maximum by using ethanol and NaOH as sacrificial reagent because CdS shows photocorrosion in acidic medium so it works well in basic media.

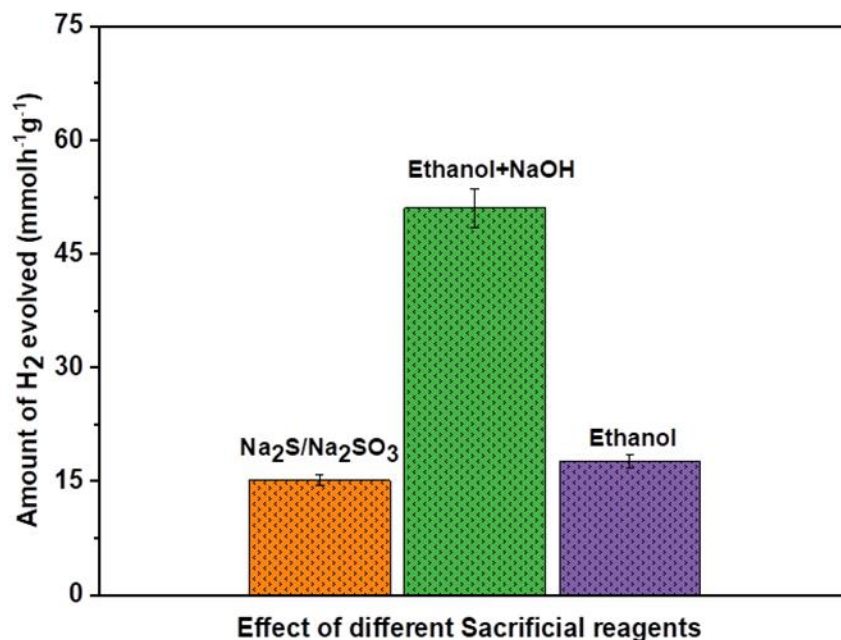


Figure 31: H₂ production over different sacrificial reagents

5.4 Chronoamperometry:

A potent method for examining the charge recombination and light response of materials is chronoamperometric chopping (CA). In the instance of the Mxene, α -Fe₂O₃ and CdS composite, the photocurrent response of the Mxene/ α -Fe₂O₃/CdS heterostructure in a 0.5 M Na₂S solution under chopping irradiation at 0.5 V was examined using the CA technique. It was decided to chop every 100 seconds at a mild off-on pace. The results demonstrate that the composite material had a substantially higher photocurrent density of 55mA/cm² than its pristine materials, Mxene, α -Fe₂O₃ and CdS.

This increase in photocurrent density suggests that Mxene/ α -Fe₂O₃/CdS the heterojunction system's photogenerated charge transport and separation processes are extremely effective.

The composite material additionally had an improved current density in the dark, further demonstrating improved charge transport and separation. The CA analysis supports Mxene/ α -Fe₂O₃/CdS heterojunction system's ability to efficiently promote charge separation and transport, which is crucial for applications in photovoltaic devices and photocatalysis.

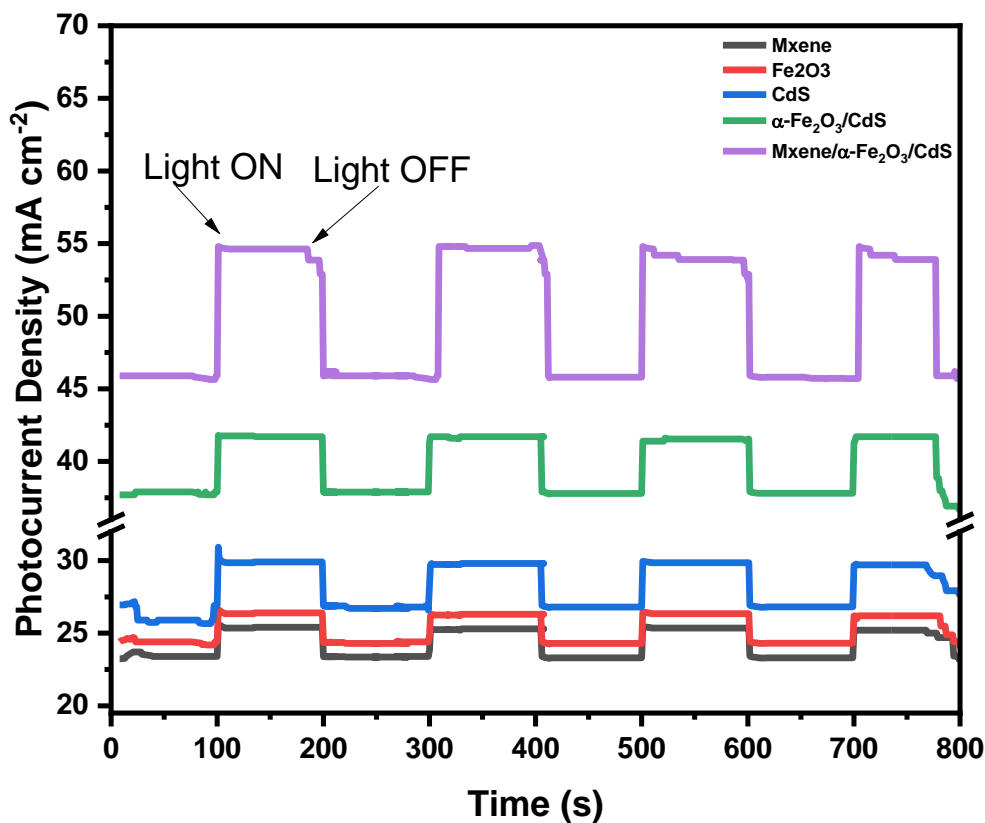


Figure 32 : CA at 0.5V DC supply

5.5 Proposed Mechanism:

The heterojunction contains a built-in electric field that makes it easier for photoinduced electrons and holes to be separated and transported, which is required for photocatalytic reactions such as reduction of O₂ to •O₂ and the oxidation of H₂O to •OH. The electric field is produced as a result

of the passage of electrons from $\alpha\text{-Fe}_2\text{O}_3$ to CdS, which forms a reduction layer on the CdS side and an electron-rich zone on the $\alpha\text{-Fe}_2\text{O}_3$ side

The transport of holes on the VB of CdS and the transport of electrons on the CB of $\alpha\text{-Fe}_2\text{O}_3$ towards the interface may be facilitated by the polarization of the electrical double layer and the concentration of charge carriers at the interface, which may result in a bending up/down of VB maximum and CB minimum. By conserving the holes on the VB of $\alpha\text{-Fe}_2\text{O}_3$ and the electrons on the CB of CdS, this enables the effective recombination of photoinduced electrons and holes. Additionally, the release of oxidative holes on the VB of CdS during recombination may lessen the oxidation of S^{2-} ions within the structure, stabilizing the substance. Moreover Mxene is used as cocatalyst. The Schottky barrier is created at the Mxene and CdS interfaces by the presence of mxene cocatalysts over CdS surfaces. The Schottky barrier prevents electron backflow and decreases the H ions to form H_2 . H_2 production is increased by this efficient synergism between cocatalysts with $\alpha\text{-Fe}_2\text{O}_3$ and Mxene (Schottky junctions) across the CdS surfaces without charge recombination or quasi-Fermi level splitting.

Proposed Mechanism

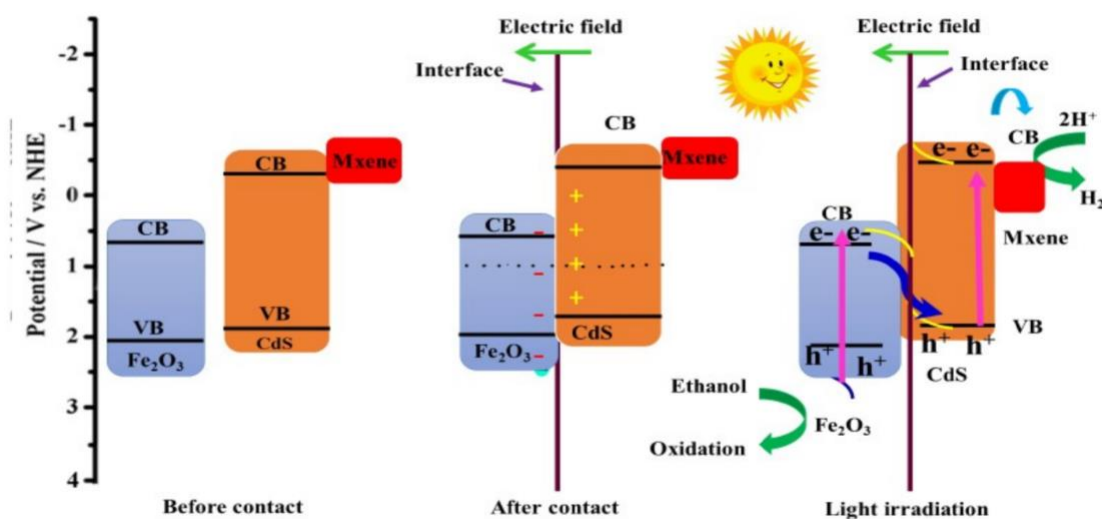


Figure 33: Mechanism of photocatalytic water splitting showing C-B, V-B and Fermi level.

6 Conclusions

A significant advance in the production of hydrogen has been made possible by the effective synthesis of Mxene/ α -Fe₂O₃/CdS the photocatalyst. The exceptional efficiency of this newly created photocatalyst is attested to by the impressive rate of 51 mmol g⁻¹ h⁻¹. The thorough examination using SEM, TEM, EDX, HAADF and chronoamperometry not only supports the significant hydrogen production but also the compositional and structural integrity of the created material. These results represent an important step towards efficient and long-lasting hydrogen generation. Mxene, α -Fe₂O₃, and CdS together demonstrate the potential for developing photocatalytic materials for improved energy conversion applications. This accomplishment paves the path for additional innovation and research in the field of renewable energy, helping to create a more energy-efficient and sustainable future.

7 References:

1. Maginn, E.J., *What to Do with CO₂*. 2010, ACS Publications. p. 3478-3479.
2. Smol, J.P., *Climate Change: A planet in flux*. Nature, 2012. **483**(7387): p. S12-S15.
3. Chakraborty, S., et al., *An efficient nickel catalyst for the reduction of carbon dioxide with a borane*. Journal of the American Chemical Society, 2010. **132**(26): p. 8872-8873.
4. Ziebart, C., et al., *Well-defined iron catalyst for improved hydrogenation of carbon dioxide and bicarbonate*. Journal of the American Chemical Society, 2012. **134**(51): p. 20701-20704.
5. Kočí, K., L. Obalová, and Z. Lacný, *Photocatalytic reduction of CO₂ over TiO₂ based catalysts*. Chemical Papers, 2008. **62**(1): p. 1-9.
6. Fujishima, A. and K. Honda, *Electrochemical photolysis of water at a semiconductor electrode*. nature, 1972. **238**(5358): p. 37-38.
7. Fujishima, A., T.N. Rao, and D.A. Tryk, *Titanium dioxide photocatalysis*. Journal of photochemistry and photobiology C: Photochemistry reviews, 2000. **1**(1): p. 1-21.
8. Kurihara, K. and J.H. Fendler, *Electron-transfer catalysis by surfactant vesicle stabilized colloidal platinum*. Journal of the American Chemical Society, 1983. **105**(19): p. 6152-6153.
9. Ma, Y., et al., *Titanium dioxide-based nanomaterials for photocatalytic fuel generations*. Chemical reviews, 2014. **114**(19): p. 9987-10043.
10. Katsumata, K.-i., et al., *Photocatalytic activity of NaNbO₃ thin films*. Journal of the American Chemical Society, 2009. **131**(11): p. 3856-3857.
11. Hoang, A.T., et al., *Hydrogen production by water splitting with support of metal and carbon-based photocatalysts*. ACS Sustainable Chemistry & Engineering, 2023. **11**(4): p. 1221-1252.
12. Dellamatrice, P.M., et al., *Degradation of textile dyes by cyanobacteria*. brazilian journal of microbiology, 2017. **48**: p. 25-31.
13. Gümüş, D. and F. Akbal, *Photocatalytic degradation of textile dye and wastewater*. Water, Air, & Soil Pollution, 2011. **216**: p. 117-124.
14. Nagajyothi, P.C., et al., *Green synthesis: Photocatalytic degradation of textile dyes using metal and metal oxide nanoparticles-latest trends and advancements*. Critical Reviews in Environmental Science and Technology, 2020. **50**(24): p. 2617-2723.
15. Chen, X., et al., *Semiconductor-based photocatalytic hydrogen generation*. Chemical reviews, 2010. **110**(11): p. 6503-6570.
16. Afroz, K., et al., *A heterojunction strategy to improve the visible light sensitive water splitting performance of photocatalytic materials*. Journal of Materials Chemistry A, 2018. **6**(44): p. 21696-21718.
17. Moniruddin, M., et al., *Hierarchically 3D assembled strontium titanate nanomaterials for water splitting application*. Applied Surface Science, 2017. **419**: p. 886-892.
18. Liu, Z., et al., *Plasmon resonant enhancement of photocatalytic water splitting under visible illumination*. Nano letters, 2011. **11**(3): p. 1111-1116.
19. Septina, W., et al., *Stabilized solar hydrogen production with CuO/CdS heterojunction thin film photocathodes*. Chemistry of Materials, 2017. **29**(4): p. 1735-1743.

20. Charanpahari, A., et al., *Enhanced photocatalytic activity of multi-doped TiO₂ for the degradation of methyl orange*. Applied Catalysis A: General, 2012. **443**: p. 96-102.
21. Kim, E.S., et al., *Fabrication of CaFe₂O₄/TaON heterojunction photoanode for photoelectrochemical water oxidation*. Journal of the American Chemical Society, 2013. **135**(14): p. 5375-5383.
22. Reece, S.Y., et al., *Wireless solar water splitting using silicon-based semiconductors and earth-abundant catalysts*. Science, 2011. **334**(6056): p. 645-648.
23. Sun, K., et al., *3D branched nanowire heterojunction photoelectrodes for high-efficiency solar water splitting and H₂ generation*. Nanoscale, 2012. **4**(5): p. 1515-1521.
24. Hou, Y., et al., *Visible light-driven α -Fe₂O₃ nanorod/graphene/BiV_{1-x}Mo_xO₄ core/shell heterojunction array for efficient photoelectrochemical water splitting*. Nano Letters, 2012. **12**(12): p. 6464-6473.
25. Xiang, Q., J. Yu, and M. Jaroniec, *Preparation and enhanced visible-light photocatalytic H₂-production activity of graphene/C₃N₄ composites*. The Journal of Physical Chemistry C, 2011. **115**(15): p. 7355-7363.
26. Dong, F., et al., *In situ construction of g-C₃N₄/g-C₃N₄ metal-free heterojunction for enhanced visible-light photocatalysis*. ACS Applied Materials & Interfaces, 2013. **5**(21): p. 11392-11401.
27. Tian, Y., et al., *Hydrothermal synthesis of graphitic carbon nitride–Bi₂WO₆ heterojunctions with enhanced visible light photocatalytic activities*. ACS Applied Materials & Interfaces, 2013. **5**(15): p. 7079-7085.
28. Kudo, A. and Y. Miseki, *Heterogeneous photocatalyst materials for water splitting*. Chemical Society Reviews, 2009. **38**(1): p. 253-278.
29. Low, J., et al., *Heterojunction photocatalysts*. Advanced Materials, 2017. **29**(20): p. 1601694.
30. Meng, X., et al., *Boosting hydrogen evolution performance of a CdS-based photocatalyst: in situ transition from type I to type II heterojunction during photocatalysis*. ACS Catalysis, 2022. **12**(16): p. 10115-10126.
31. Guo, L., et al., *Morphology engineering of type-II heterojunction nanoarrays for improved sonophotocatalytic capability*. Ultrasonics Sonochemistry, 2021. **81**: p. 105849.
32. Schuettfort, T., A. Nish, and R.J. Nicholas, *Observation of a type II heterojunction in a highly ordered polymer–carbon nanotube nanohybrid structure*. Nano Letters, 2009. **9**(11): p. 3871-3876.
33. Mikhailova, M. and A. Titkov, *Type II heterojunctions in the GaInAsSb/GaSb system*. Semiconductor Science and Technology, 1994. **9**(7): p. 1279.
34. Que, M., et al., *Recent advances in g-C₃N₄ composites within four types of heterojunctions for photocatalytic CO₂ reduction*. Nanoscale, 2021. **13**(14): p. 6692-6712.
35. Bantí-Barcenas, J., F. Sutará, and I. Hernández-Calderón. *Design of a quantum well based on a ZnCdSe/ZnTe type II heterostructure confined type I within ZnSe barriers*. in AIP Conference Proceedings. 2018. AIP Publishing.
36. Wu, E., et al., *In situ fabrication of 2D WS₂/Si type-II heterojunction for self-powered broadband photodetector with response up to mid-infrared*. ACS Photonics, 2019. **6**(2): p. 565-572.
37. Zhang, Z., et al., *Electrospun nanofibers of p-type NiO/n-type ZnO heterojunctions with enhanced photocatalytic activity*. ACS Applied Materials & Interfaces, 2010. **2**(10): p. 2915-2923.

38. Xu, Q., et al., *S-scheme heterojunction photocatalyst*. Chem, 2020. **6**(7): p. 1543-1559.
39. Malik, R., et al., *Dissimilar dimensional materials based tailored heterostructures for photocatalytic hydrogen production*. Renewable and Sustainable Energy Reviews, 2023. **181**: p. 113348.
40. Chava, R.K., J.Y. Do, and M. Kang, *Enhanced photoexcited carrier separation in CdS–SnS 2 heteronanostructures: A new 1D–0D visible-light photocatalytic system for the hydrogen evolution reaction*. Journal of Materials Chemistry A, 2019. **7**(22): p. 13614-13628.
41. Sultana, S., S. Mansingh, and K. Parida, *Crystal facet and surface defect engineered low dimensional CeO₂ (0D, 1D, 2D) based photocatalytic materials towards energy generation and pollution abatement*. Materials Advances, 2021. **2**(21): p. 6942-6983.
42. Abbas, M., et al., *Agri-nanotechnology and tree nanobionics: Augmentation in crop yield, biosafety, and biomass accumulation*. Frontiers in bioengineering and biotechnology, 2022. **10**: p. 853045.
43. Wang, Y., et al., *Designing a 0D/1D s-scheme heterojunction of cadmium selenide and polymeric carbon nitride for photocatalytic water splitting and carbon dioxide reduction*. Molecules, 2022. **27**(19): p. 6286.
44. Lee, J.-W., et al., *Photoelectrochemical water splitting using one-dimensional nanostructures*. Journal of Materials Chemistry A, 2021. **9**(38): p. 21576-21606.
45. Xiao, R., et al., *In situ fabrication of 1D CdS nanorod/2D Ti₃C₂ MXene nanosheet Schottky heterojunction toward enhanced photocatalytic hydrogen evolution*. Applied Catalysis B: Environmental, 2020. **268**: p. 118382.
46. Jiang, H., et al., *Two-dimensional materials: From mechanical properties to flexible mechanical sensors*. InfoMat, 2020. **2**(6): p. 1077-1094.
47. Albero, J., D. Mateo, and H. García, *Graphene-based materials as efficient photocatalysts for water splitting*. Molecules, 2019. **24**(5): p. 906.
48. Li, J., et al., *Graphene and their hybrid electrocatalysts for water splitting*. ChemCatChem, 2017. **9**(9): p. 1554-1568.
49. Wang, F., et al., *Recent advances in transition-metal dichalcogenide based nanomaterials for water splitting*. Nanoscale, 2015. **7**(47): p. 19764-19788.
50. Yuan, Y.-J., et al., *Role of two-dimensional nanointerfaces in enhancing the photocatalytic performance of 2D-2D MoS₂/CdS photocatalysts for H₂ production*. Chemical Engineering Journal, 2018. **350**: p. 335-343.
51. Li, S., Y. Zhang, and H. Huang, *Black phosphorus-based heterostructures for photocatalysis and photoelectrochemical water splitting*. Journal of Energy Chemistry, 2022. **67**: p. 745-779.
52. Wang, G., et al., *A two-dimensional h-BN/C 2 N heterostructure as a promising metal-free photocatalyst for overall water-splitting*. Physical Chemistry Chemical Physics, 2020. **22**(42): p. 24446-24454.
53. Yu, Z., et al., *Interfacial charge transport in 1D TiO₂ based photoelectrodes for photoelectrochemical water splitting*. Small, 2021. **17**(9): p. 1903378.
54. Fu, H.Q., et al., *1D/1D hierarchical nickel sulfide/phosphide nanostructures for electrocatalytic water oxidation*. ACS Energy Letters, 2018. **3**(9): p. 2021-2029.
55. Gupta, U. and C. Rao, *Hydrogen generation by water splitting using MoS₂ and other transition metal dichalcogenides*. Nano Energy, 2017. **41**: p. 49-65.

56. Liu, Y., et al., *Nitrogen doped graphene quantum dots as a cocatalyst of SrTiO₃ (Al)/CoO_x for photocatalytic overall water splitting*. *Catalysis Science & Technology*, 2021. **11**(9): p. 3039-3046.
57. Meng, J., et al., *Recent progress in synthesis, properties, and applications of hexagonal boron nitride-based heterostructures*. *Nanotechnology*, 2018. **30**(7): p. 074003.
58. Huang, J., et al., *Anchoring of 2D CdS on Nb₂CTX MXene nanosheets for boosting photocatalytic H₂ evolution*. *Journal of Alloys and Compounds*, 2022. **923**: p. 166256.
59. Ding, M., et al., *Evidencing interfacial charge transfer in 2D CdS/2D MXene Schottky heterojunctions toward high-efficiency photocatalytic hydrogen production*. *Solar Rrl*, 2021. **5**(2): p. 2000414.
60. Ning, X. and G. Lu, *Photocorrosion inhibition of CdS-based catalysts for photocatalytic overall water splitting*. *Nanoscale*, 2020. **12**(3): p. 1213-1223.
61. Guo, Z., et al., *MXene: a promising photocatalyst for water splitting*. *Journal of Materials Chemistry A*, 2016. **4**(29): p. 11446-11452.
62. Qiao, J., et al., *Research progress of MXene-based catalysts for electrochemical water-splitting and metal-air batteries*. *Energy Storage Materials*, 2021. **43**: p. 509-530.
63. Yue, Q., et al., *Hierarchical mesoporous MXene–NiCoP electrocatalyst for water-splitting*. *ACS applied materials & interfaces*, 2020. **12**(16): p. 18570-18577.
64. Lv, Z., et al., *Induction of Co₂P Growth on a MXene (Ti₃C₂T_x)-Modified Self-Supporting Electrode for Efficient Overall Water Splitting*. *The Journal of Physical Chemistry Letters*, 2021. **12**(20): p. 4841-4848.
65. Zhang, H., et al., *Preparation of magnetic α -Fe₂O₃/ZnFe₂O₄@ Ti₃C₂ MXene with excellent photocatalytic performance*. *Ceramics International*, 2020. **46**(1): p. 81-88.
66. Yao, C., et al., *2D/2D α -Fe₂O₃/single-layer MXene Schottky photocatalysis-PMS activation bidirectionally enhanced coupling system for environmental remediation*. *Journal of Alloys and Compounds*, 2023. **941**: p. 168920.
67. Ye, R.-K., et al., *Surface engineering of hematite nanorods by 2D Ti₃C₂-MXene: Suppressing the electron-hole recombination for enhanced photoelectrochemical performance*. *Applied Catalysis B: Environmental*, 2021. **291**: p. 120107.
68. Baldovi, H.G., *Optimization of α -Fe₂O₃ nanopillars diameters for photoelectrochemical enhancement of α -Fe₂O₃-TiO₂ heterojunction*. *Nanomaterials*, 2021. **11**(8): p. 2019.
69. Shuai, T.-Y., et al., *Recent developments of MXene-based catalysts for hydrogen production by water splitting*. *Green Chemistry*, 2023.
70. Sherryrna, A. and M. Tahir, *Role of Ti₃C₂ MXene as prominent schottky barriers in driving hydrogen production through photoinduced water splitting: a comprehensive review*. *ACS Applied Energy Materials*, 2021. **4**(11): p. 11982-12006.
71. Gogoi, D., et al., *Silver grafted graphitic-carbon nitride ternary hetero-junction Ag/gC₃N₄ (Urea)-gC₃N₄ (Thiourea) with efficient charge transfer for enhanced visible-light photocatalytic green H₂ production*. *Applied Surface Science*, 2021. **558**: p. 149900.
72. Wang, Q., et al., *Construction of Bi-assisted modified CdS/TiO₂ nanotube arrays with ternary S-scheme heterojunction for photocatalytic wastewater treatment and hydrogen production*. *Fuel*, 2022. **322**: p. 124163.
73. Ahmet, I.Y., et al., *Planar and Nanostructured n-Si/Metal-Oxide/WO₃/BiVO₄ Monolithic Tandem Devices for Unassisted Solar Water Splitting*. *Advanced Energy and Sustainability Research*, 2020. **1**(2): p. 2000037.

74. Wang, Y., et al., *Bi-quantum dots co-sensitized TiO₂ nanocomposites: Templated synthesis and stabilized by polymer brushes*. *Materials Chemistry and Physics*, 2012. **134**(2-3): p. 966-972.
75. Wang, M., et al., *Facile synthesis of MoS₂/g-C₃N₄/GO ternary heterojunction with enhanced photocatalytic activity for water splitting*. *ACS Sustainable Chemistry & Engineering*, 2017. **5**(9): p. 7878-7886.
76. Farhoosh, S., et al., *Newly designed ternary hematite-based heterojunction for PEC water splitting*. *Applied Surface Science*, 2021. **550**: p. 149374.
77. Li, Y., et al., *An effective CdS/Ti-Fe₂O₃ heterojunction photoanode: Analyzing Z-scheme charge-transfer mechanism for enhanced photoelectrochemical water-oxidation activity*. *Chinese Journal of Catalysis*, 2021. **42**(5): p. 762-771.
78. Shen, R., et al., *Integrating 2D/2D CdS/ α -Fe₂O₃ ultrathin bilayer Z-scheme heterojunction with metallic β -NiS nanosheet-based ohmic-junction for efficient photocatalytic H₂ evolution*. *Applied Catalysis B: Environmental*, 2020. **266**: p. 118619.
79. Natarajan, K., M. Saraf, and S.M. Mobin, *Visible-light-induced water splitting based on a novel α -Fe₂O₃/CdS heterostructure*. *ACS omega*, 2017. **2**(7): p. 3447-3456.
80. Guo, F., et al., *CdS nanoparticles decorated hexagonal Fe₂O₃ nanosheets with a Z-scheme photogenerated electron transfer path for improved visible-light photocatalytic hydrogen production*. *Chinese Journal of Chemical Engineering*, 2022. **43**: p. 266-274.
81. Yavuz, C. and S. Erten-Ela, *Solar light-responsive α -Fe₂O₃/CdS/g-C₃N₄ ternary photocatalyst for photocatalytic hydrogen production and photodegradation of methylene blue*. *Journal of Alloys and Compounds*, 2022. **908**: p. 164584.
82. Liu, X., et al., *Optimizing the reaction pathway by active site regulation in the CdS/Fe₂O₃ Z-scheme heterojunction system for highly selective photocatalytic benzylamine oxidation integrated with H₂ production*. *ACS Catalysis*, 2022. **12**(19): p. 12386-12397.
83. Alfaifi, B.Y., et al., *Photoelectrochemical solar water splitting: From basic principles to advanced devices*. 2018.
84. Yu, J., et al., *Morphology-dependent photocatalytic H₂-production activity of CdS*. *Applied Catalysis B: Environmental*, 2014. **156**: p. 184-191.
85. Simon, T., et al., *Redox shuttle mechanism enhances photocatalytic H₂ generation on Ni-decorated CdS nanorods*. *Nature materials*, 2014. **13**(11): p. 1013-1018.
86. Wang, Q., et al., *Photochemical preparation of Cd/CdS photocatalysts and their efficient photocatalytic hydrogen production under visible light irradiation*. *Green Chemistry*, 2014. **16**(5): p. 2728-2735.
87. Zeng, P., et al., *One-pot synthesis of reduced graphene oxide-cadmium sulfide nanocomposite and its photocatalytic hydrogen production*. *Physical Chemistry Chemical Physics*, 2011. **13**(48): p. 21496-21502.
88. Lang, D., T. Shen, and Q. Xiang, *Roles of MoS₂ and graphene as cocatalysts in the enhanced visible-light photocatalytic H₂ production activity of multiarmed CdS nanorods*. *ChemCatChem*, 2015. **7**(6): p. 943-951.
89. Mao, N., *Investigating the heteronjunction between ZnO/Fe₂O₃ and g-C₃N₄ for an enhanced photocatalytic H₂ production under visible-light irradiation*. *Scientific reports*, 2019. **9**(1): p. 12383.
90. Carraro, G., et al., *Enhanced hydrogen production by photoreforming of renewable oxygenates through nanostructured Fe₂O₃ polymorphs*. *Advanced Functional Materials*, 2014. **24**(3): p. 372-378.

91. Li, Y., et al., *Synergetic effect of defects rich MoS₂ and Ti₃C₂ MXene as cocatalysts for enhanced photocatalytic H₂ production activity of TiO₂*. Chemical Engineering Journal, 2020. **383**: p. 123178.
92. Yin, J., et al., *Facile preparation of self-assembled MXene@ Au@ CdS nanocomposite with enhanced photocatalytic hydrogen production activity*. Sci. China Mater, 2020. **63**(11): p. 2228-2238.
93. Wang, Y., et al., *Ti₃C₂ MXene coupled with CdS nanoflowers as 2D/3D heterostructures for enhanced photocatalytic hydrogen production activity*. International Journal of Hydrogen Energy, 2022. **47**(52): p. 22045-22053.